

Banner appropriate to article type will appear here in typeset article

# Covariant algebraic Reynolds stress modelling of curvature effects in high-Reynolds-number Taylor–Couette turbulence

Kazuhiro Inagaki<sup>1</sup>† and Yasufumi Horimoto<sup>2</sup>

<sup>1</sup>Department of Mechanical Engineering, Doshisha University, Kyotanabe 610-0394, Japan

<sup>2</sup>Laboratory for Flow Control, Faculty of Engineering, Hokkaido University, Hokkaido 060-8628, Japan

(Received xx; revised xx; accepted xx)

Generally covariant expressions of algebraic Reynolds stress models (ARSMs) for rotating or curved turbulent flows have been discussed. Nearly constant mean angular momentum profiles, which are widely observed in curved turbulent flows including the bulk region of Taylor–Couette (TC) flows, are employed to evaluate the performance of Reynolds-averaged Navier–Stokes (RANS) models. For high-Reynolds-number TC flows where the inner and outer cylinders are weakly counter-rotating and co-rotating, both the bulk and boundary layers become turbulent without Taylor rolls, referred to as the featureless ultimate regime (UR). Thus, we can examine the RANS models as a one-dimensional problem in the featureless UR of the TC turbulence. High-Reynolds-number experiments of TC turbulence are performed for reference, where the radius ratio is  $\eta = r_{\text{in}}/r_{\text{out}} = 0.732$  and the angular velocity ratio  $a = -\omega_{\text{out}}/\omega_{\text{in}}$  is in the range  $-0.5 \leq a \leq 0.1$ . Verification of the RANS based on the conventional ARSM suggests that convection of the Reynolds stress is essential for predicting the angular momentum profile. We introduce the Jaumann derivative as a covariant time derivative to develop ARSMs that incorporate the convection effect in a covariant manner. The proposed ARSM using the Jaumann derivative of the term composed of the strain and vorticity tensors successfully predicts the nearly constant mean angular momentum for a wide range of angular velocity ratios in the co-rotating case. The modelling approach incorporating time-derivative terms is a candidate for expressing curvature effects while satisfying the covariance of the Reynolds stress tensor.

## 1. Introduction

Mathematical properties of equations are one of the significant constraints in modelling physical phenomena. For turbulence modelling, the importance of form invariance or covariance of constitutive relations has been claimed (Weis & Hutter 2003; Hamba 2006a; Speziale 1979; Frewer 2009; Ariki 2015a). Particularly, Frewer (2009) and Ariki (2015a) discussed the general covariance of constitutive relations in turbulence models. In contrast to the Euclidean covariance (e.g Weis & Hutter 2003; Hamba 2006a), the general covariance includes the transformation into the curvilinear or stretching coordinate system, which can be time-dependent. Even though the equation of motion is not frame-independent,

† Email address for correspondence: kinagaki@mail.doshisha.ac.jp

as represented by the Coriolis force emerging in a rotating frame, constitutive relations can be covariant. Mathematically, any tensors are covariant. Covariance is characterised by a transformation property of the quantity between two coordinate systems. Namely, when we consider two different coordinates  $(t, \mathbf{x})$  and  $(\tilde{t}, \tilde{\mathbf{x}})$ , tensor quantities in each system,  $\tilde{A}^{ij\dots}_{\ell m\dots} = \tilde{A}^{ij\dots}_{\ell m\dots}(\tilde{\mathbf{x}}, \tilde{t})$  and  $A^{ij\dots}_{\ell m\dots} = A^{ij\dots}_{\ell m\dots}(\mathbf{x}, t)$ , must satisfy the following relation:

$$\tilde{A}^{ab\dots}_{cd\dots}(\tilde{t}, \tilde{\mathbf{x}}) = \frac{\partial \tilde{x}^a}{\partial x^i} \frac{\partial \tilde{x}^b}{\partial x^j} \cdots \frac{\partial x^\ell}{\partial \tilde{x}^c} \frac{\partial x^m}{\partial \tilde{x}^d} \cdots A^{ij\dots}_{\ell m\dots}(t, \mathbf{x}). \quad (1.1)$$

Here, the superscripts and subscripts denote the contravariant and covariant components, respectively. They can be transformed as  $A^i = g^{ij} A_j$  or  $A_i = g_{ij} A^j$  via the metric tensor  $g^{ij}$ . The Reynolds stress tensor in Reynolds-averaged Navier-Stokes (RANS) modelling also satisfies the relation (1.1) (Speziale 1979; Frewer 2009; Ariki 2015a). Violation of the covariance of the Reynolds stress decreases the physical reliability of the turbulence models. Hence, the covariance of Reynolds stress is important for assessing the physical properties of RANS models (Speziale 1979; Frewer 2009; Ariki 2015a, 2017). It was shown that considering the conservation laws or symmetries in expansion, rotation, and translation improves the accuracy of machine-learning-based numerical simulation of partial differential equations (Horie & Mitsume 2024). For turbulence modelling, the mathematical constraints such as the covariance or realisability conditions (positiveness of squared quantities and Schwartz's inequality for second moments) are strong guiding principles for data-driven approaches, which improve the accuracy of resulting models (Ling *et al.* 2016; Wu *et al.* 2018; Duraisamy *et al.* 2019; Jiang *et al.* 2021). Studying the mathematical structure of turbulence models paves the way for further developments in turbulence modelling even in the age of data science.

Algebraic Reynolds stress modelling (ARSM) is a basic way of constructing a model for Reynolds stress in RANS modelling (Pope 2000; Durbin 2018). The weak-equilibrium assumption is often employed to obtain a constitutive relation for the Reynolds stress. Namely, for the Reynolds stress anisotropy tensor  $\tilde{b}^{ij} = \tilde{b}^{ij}(\tilde{t}, \tilde{\mathbf{x}})$  (hereafter, anisotropy tensor) and mean velocity  $\tilde{U}^i(\tilde{t}, \tilde{\mathbf{x}})$  in a  $(\tilde{t}, \tilde{\mathbf{x}})$  system,

$$\left( \frac{\partial}{\partial \tilde{t}} + \tilde{U}^\ell(\tilde{t}, \tilde{\mathbf{x}}) \frac{\partial}{\partial \tilde{x}^\ell} \right) \tilde{b}^{ij}(\tilde{t}, \tilde{\mathbf{x}}) = 0 \quad (1.2)$$

is assumed. The anisotropy tensor is defined later in §2.3.1. The conventional way of constructing the ARSMs in rotating or curved turbulent flows is to find the coordinate system  $(\tilde{t}, \tilde{\mathbf{x}})$  that is assumed to satisfy the weak-equilibrium assumption (1.2) (Girimaji 1997; Gatski & Jongen 2000; Wallin & Johansson 2002; Gatski & Wallin 2004). Girimaji (1997) assumed that the anisotropy tensor is constant along the mean streamline and proposed the acceleration coordinate as a Galilean invariant proxy of the local streamline coordinate. Gatski & Jongen (2000) and Wallin & Johansson (2002) employed the principal axis of the mean strain-rate tensor as another proxy coordinate. Hamba (2006a) suggested that the ARSM can be covariant when considering the Euclidean transformation, i.e. rotation and translation transformation of coordinate systems. Notably, the accuracy of these ARSMs for rotating or curved turbulent flows directly depends on the choice of the coordinate system where the weak-equilibrium condition is assumed to be satisfied. The ARSMs based on the weak-equilibrium assumption are not unique because of the differences between the selected proxy coordinates, and their assessment has not yet been completed (Brethouwer 2022). Abe (2019) performed numerical simulations of separating turbulent flows and showed that the convection term becomes prominent in the Reynolds shear stress budget, which suggests that the anisotropy tensor may not be constant along the streamline owing to the strong flow

curvature. Furthermore, we cannot find the coordinate system in which the weak-equilibrium assumption holds for the periodically sheared turbulent flows because the phase of the mean strain rate and Reynolds shear stress and the period of the Reynolds normal and shear stresses are different, respectively (Yu & Girimaji 2006; Hamlington & Dahm 2008; Ariki & Ikeda 2023). Hence, the expression of curvature or rotation effects in ARSM remains to be discussed.

It is valuable to consider an alternative modelling approach that does not employ the weak-equilibrium assumption. In this study, we adopt an approach that explicitly employs a time derivative of tensors, such as the strain rate (Yoshizawa 1984; Speziale 1987; Ahmadi & Chowdhury 1991; Taulbee 1992; Hamlington & Dahm 2008; Ariki 2019; Ariki & Ikeda 2023). Hamba (2006*b*) employed the Lagrangian or material derivative in a rotating frame, particularly the derivative of a tensor composed of the strain-rate and absolute-vorticity tensors for predicting the nearly zero mean absolute vorticity profiles in the spanwise rotating turbulent channel flows. Spalart & Shur (1997) proposed a scalar measure of the curvature effects in three-dimensional flows using the Lagrangian derivative of the strain-rate tensor. If we employ a covariant time derivative such as the Oldroyd or convective derivative (Oldroyd 1950; Thiffeault 2001), we can develop generally covariant algebraic turbulence models (Speziale 1987; Ariki 2015*a*, 2019; Ariki & Ikeda 2023). This study employs the Taylor–Couette (TC) flow as a simple example of curved turbulent flows to construct and validate the turbulence model using covariant time derivatives.

The TC flow, which is driven by the friction of two independently rotating concentric cylinders, has long been examined for studying the effects of rotation or flow curvature on turbulence. For relatively low Reynolds numbers based on the rotations of the cylinders and gap width, the TC flow exhibits abundant flow dynamics, including developed bulk turbulence (Coles 1965; Andereck *et al.* 1986; Chossat & Iooss 1994). For high-Reynolds-number turbulence, we can refer to a pioneering experiment by Wendt (1933). Over the last two decades, exploration of high-Reynolds-number TC turbulence has progressed both experimentally and numerically (Grossmann *et al.* 2016). At sufficiently high Reynolds numbers, both the bulk and boundary layers on the cylinders become turbulent (van Hout & Katz 2011; Huisman *et al.* 2013; Ostilla-Mónico *et al.* 2014*a,b,c*; Chouippe *et al.* 2014; Berghout *et al.* 2020). This high-Reynolds-number regime with turbulent boundary layers is referred to as the ultimate regime (UR). Furthermore, for cases in which two cylinders are weakly counter-rotating and co-rotating, the so-called Taylor rolls vanish; thus, the flows lead to a featureless UR (Ostilla-Mónico *et al.* 2014*c*). Featureless turbulence with co-rotating inner and outer boundaries is often studied in the context of angular momentum transport in astrophysical objects such as accretion disks (Dubrulle *et al.* 2005; Schartman *et al.* 2009; Ji & Balbus 2013). For the featureless UR, the statistics of TC flow yield one-dimensional as a function of radial position. Such one-dimensional statistics of turbulent flows may be predicted using a relatively simple RANS model.

Curved or rotating turbulent flows exhibit characteristic mean velocity profiles. For turbulent TC flows, a nearly constant mean angular momentum appears in the bulk region, as shown in previous experiments (Smith & Townsend 1982; Lewis & Swinney 1999; Froitzheim *et al.* 2017; Ezeta *et al.* 2018), numerical simulations (Dong 2007; Brauckmann & Eckhardt 2013; Brauckmann *et al.* 2016; Froitzheim *et al.* 2019; Cheng *et al.* 2020), and theoretical analysis (Deguchi 2023). Brauckmann *et al.* (2016) showed that the nearly constant mean angular momentum is robust to a wide range of angular velocity ratios of the outer cylinder to the inner cylinder and is observed for weakly counter-rotating and co-rotating cases. A nearly constant mean angular momentum was also observed in curved channel flows with strong curvature (Wattendorf 1935; Nagata & Kasagi 2004; Brethouwer 2022). A similar characteristic statistical property of rotating turbulent flows is the nearly zero

mean absolute vorticity (Johnston *et al.* 1972; Tanaka *et al.* 2000; Hamba 2006*b*; Grundestam *et al.* 2008; Xia *et al.* 2016; Kawata & Alfredsson 2016*a*). Both the constant mean angular momentum and zero mean absolute vorticity conform to neutral stability (Cambon *et al.* 1994; Brauckmann *et al.* 2016; Brethouwer 2022). Predicting the nearly zero mean absolute vorticity has been a good benchmark for RANS modelling because it cannot be reproduced using standard eddy-viscosity models (Gatski & Speziale 1993; Wallin & Johansson 2000, 2002; Gatski & Wallin 2004; Hamba 2006*b*). This study investigates the essential model expression in ARSMs for predicting the nearly constant mean angular momentum in the featureless UR of the TC turbulence.

The remainder of this paper is organised as follows. In §2, we summarise the basic equations for the mean velocity and Reynolds stress, and transformation rules of the related terms. In this section, we discuss the covariance of turbulence models and their importance based on previous studies. We also derive an ARSM involving the flow curvature effects in cylindrical coordinates. The performance of the ARSMs is discussed and compared with experimental results for the featureless UR of the TC turbulence in §3. We discuss the covariant expression of the curvature effects of Reynolds stress in §4. The physical properties of the derived model are also discussed. The conclusions are presented in §5.

## 2. Curvature effects in basic equations

### 2.1. Governing equations

The continuity and the  $i$ th contravariant component of the Navier–Stokes equations for incompressible flows in an inertial frame are as follows (Frewer 2009; Ariki 2015*a*; Kajishima & Taira 2017):

$$\nabla_i u^i = 0, \quad (2.1)$$

$$\frac{\partial u^i}{\partial t} = -u^j \nabla_j u^i - g^{ij} \nabla_i p + \nu g^{j\ell} \nabla_j \nabla_\ell u^i \quad (2.2)$$

where  $u^i$ ,  $p$ ,  $\nu$ , and  $g^{ij}$  denote the velocity field, pressure divided by density, kinematic viscosity, and metric tensor, respectively. Note that the operator  $\nabla_i$  denotes the covariant derivative defined as

$$\begin{aligned} \nabla_n A^{ij\dots}_{\ell m\dots} &= \frac{\partial A^{ij\dots}_{\ell m\dots}}{\partial x_m} + \Gamma_{na}^i A^{aj\dots}_{\ell m\dots} + \Gamma_{na}^j A^{ia\dots}_{\ell m\dots} + \dots \\ &\quad - \Gamma_{nl}^a A^{ij\dots}_{am\dots} - \Gamma_{nm}^a A^{ij\dots}_{\ell a\dots} - \dots, \end{aligned} \quad (2.3)$$

where

$$\Gamma_{j\ell}^i = \frac{1}{2} g^{ia} \left( \frac{\partial g_{ja}}{\partial x_\ell} + \frac{\partial g_{\ell a}}{\partial x_j} - \frac{\partial g_{j\ell}}{\partial x_a} \right) \quad (2.4)$$

is the Christoffel symbol. The covariant derivative in a cylindrical coordinate is given in Appendix A. As a result, the continuity equation and each component of the nonlinear term of the Navier–Stokes equations in cylindrical coordinates in the inertial frame can be written

as follows:

$$\nabla_i u^i = \frac{\partial u_r}{\partial r} + \frac{1}{r} \frac{\partial u_\theta}{\partial \theta} + \frac{u_r}{r} + \frac{\partial u_z}{\partial z} = \frac{1}{r} \frac{\partial}{\partial r} (r u_r) + \frac{1}{r} \frac{\partial u_\theta}{\partial \theta} + \frac{\partial u_z}{\partial z} = 0, \quad (2.5a)$$

$$\begin{aligned} u^j \nabla_j u_r &= u_r \frac{\partial u_r}{\partial r} + u_\theta \left( \frac{1}{r} \frac{\partial u_r}{\partial \theta} - \frac{u_\theta}{r} \right) + u_z \frac{\partial u_r}{\partial z} \\ &= \frac{1}{r} \frac{\partial}{\partial r} (r u_r^2) + \frac{1}{r} \frac{\partial}{\partial \theta} (u_\theta u_r) + \frac{\partial}{\partial z} (u_z u_r) - \frac{(u_\theta^2)}{r}, \end{aligned} \quad (2.5b)$$

$$\begin{aligned} u^j \nabla_j u_\theta &= u_r \frac{\partial u_\theta}{\partial r} + u_\theta \left( \frac{1}{r} \frac{\partial u_\theta}{\partial \theta} + \frac{u_r}{r} \right) + u_z \frac{\partial u_\theta}{\partial z} \\ &= \frac{1}{r} \frac{\partial}{\partial r} (r u_r u_\theta) + \frac{1}{r} \frac{\partial}{\partial \theta} (u_\theta^2) + \frac{\partial}{\partial z} (u_z u_\theta) + \frac{u_r u_\theta}{r}, \end{aligned} \quad (2.5c)$$

$$\begin{aligned} u^j \nabla_j u_z &= u_r \frac{\partial u_z}{\partial r} + u_\theta \frac{1}{r} \frac{\partial u_z}{\partial \theta} + u_z \frac{\partial u_z}{\partial z} \\ &= \frac{1}{r} \frac{\partial}{\partial r} (r u_r u_z) + \frac{1}{r} \frac{\partial}{\partial \theta} (u_\theta u_z) + \frac{\partial}{\partial z} (u_z^2). \end{aligned} \quad (2.5d)$$

Here, we consider the normalised coordinates; thus the covariant and contravariant components are equivalent. Hereafter, for the cylindrical and Cartesian coordinates, we write the components in the subscripts and do not distinguish the contravariant and covariant components. The fourth terms on the right-hand sides of (2.5b) and (2.5c) originate from the curvature of the coordinate system. This leads to flow curvature effects on the Reynolds stress.

## 2.2. Transformation rules

### 2.2.1. Velocity field and Reynolds stress

Let us consider the transformation between two coordinate systems,  $(\tilde{t}, \tilde{\mathbf{x}})$  and  $(t, \mathbf{x})$ , defined as

$$\tilde{x}^a(t, \mathbf{x}) = Q_i^a(t, \mathbf{x}) [x^i + x_0^i(t)] = \frac{\partial \tilde{x}^a}{\partial x^i} [x^i + x_0^i(t)], \quad (2.6)$$

where  $x_0^j(t)$  denotes the spatial shift of the origin, which depends only on time. We only consider the non-relativistic case where  $\tilde{t} = t$ . The transformation of velocity fields yields (Frewer 2009; Ariki 2015a)

$$\tilde{u}^a(\tilde{t}, \tilde{\mathbf{x}}) = \frac{\partial \tilde{x}^a}{\partial x^i} u^i(t, \mathbf{x}) + \frac{\partial \tilde{x}^a}{\partial t} = \frac{\partial \tilde{x}^a}{\partial x^i} \left[ u^i(t, \mathbf{x}) + \frac{dx_0^i}{dt} \right] - \tilde{\Omega}^{Fi} \tilde{x}^i, \quad (2.7)$$

where

$$\tilde{\Omega}^{Fi}{}_j = \frac{\partial \tilde{x}^i}{\partial x^\ell} \frac{\partial^2 x^\ell}{\partial t \partial \tilde{x}^j} = Q_i^\ell \frac{\partial Q^{-1\ell}{}_j}{\partial t}. \quad (2.8)$$

Note that  $Q^{-1i}{}_j$  is the inverse of  $Q^i{}_j$  that satisfies  $Q^{-1i}{}_l Q^\ell{}_j = Q^i{}_l Q^{-1\ell}{}_j = \delta_j^i$  where  $\delta_j^i (= g_j^i)$  is Kronecker's delta. In (2.7),  $dx_0^j/dt$  denotes the Galilean boost in the  $(t, \mathbf{x})$  system and  $\tilde{\Omega}^{Fi}{}_j$  denotes the rotation rate of the  $(\tilde{t}, \tilde{\mathbf{x}})$  system relative to  $(t, \mathbf{x})$  observed in the  $(\tilde{t}, \tilde{\mathbf{x}})$  system.

To derive the transformation rules for RANS, we consider the Reynolds or ensemble average:  $f = F + f'$  where  $f$  denotes basic flow variables such as  $u^i$  or  $p$ ,  $F = \langle f \rangle$ , and  $\langle \cdot \rangle$

denotes the ensemble average. The ensemble average of (2.7) yields

$$\tilde{U}^a(\tilde{t}, \tilde{\mathbf{x}}) = \frac{\partial \tilde{x}^a}{\partial x_i} U^i(t, \mathbf{x}) + \frac{\partial \tilde{x}^a}{\partial t} = \frac{\partial \tilde{x}^a}{\partial x^i} \left[ U^i(t, \mathbf{x}) + \frac{dx_0^i}{dt} \right] - \tilde{\Omega}^{\text{Fa}} \tilde{x}^i. \quad (2.9)$$

In contrast, the transformation rule for the velocity fluctuation  $u'^i$  yields

$$\tilde{u}'^a(\tilde{t}, \tilde{\mathbf{x}}) = \frac{\partial \tilde{x}^a}{\partial x_i} u'^i(t, \mathbf{x}). \quad (2.10)$$

Therefore, the transformation of the Reynolds stress  $R^{ij} = \langle u'^i u'^j \rangle$  reads

$$\tilde{R}^{ab} = \langle \tilde{u}'^a \tilde{u}'^b \rangle = \frac{\partial \tilde{x}^a}{\partial x^i} \frac{\partial \tilde{x}^b}{\partial x^j} \langle u'^i u'^j \rangle = \frac{\partial \tilde{x}^a}{\partial x^i} \frac{\partial \tilde{x}^b}{\partial x^j} R^{ij}, \quad (2.11)$$

which indicates that the Reynolds stress forms a tensor (Speziale 1979; Frewer 2009; Ariki 2015a).

### 2.2.2. Turbulence models

Turbulence modelling expresses the Reynolds stress using several tensor quantities as follows

$$R^{ij} = R^{ij}(T_{(1)}^{\ell m}, T_{(2)}^{\ell m}, \dots), \quad (2.12)$$

where  $T_{(n)}^{\ell m}$ 's are tensors, e.g. mean strain rate or absolute vorticity. If we express the Reynolds stress using a non-covariant quantity and denote it as  $R_{\text{model,NC}}^{ij} = R_{\text{model,NC}}^{ij}(T_{(1)}^{\ell m}, T_{(2)}^{\ell m}, \dots; T_{\text{NC}}^{\ell m})$ , the mathematical relation (2.11) is broken;

$$\begin{aligned} \tilde{R}_{\text{model,tr}}^{ab} &\equiv \frac{\partial \tilde{x}^a}{\partial x^i} \frac{\partial \tilde{x}^b}{\partial x^j} R_{\text{model,NC}}^{ij} = \tilde{R}_{\text{model,tr}}^{ab} \left( \tilde{T}_{(1)}^{cd}, \tilde{T}_{(2)}^{cd}, \dots; \frac{\partial \tilde{x}^c}{\partial x^\ell} \frac{\partial \tilde{x}^d}{\partial x^m} T_{\text{NC}}^{\ell m} \right) \\ &\neq \tilde{R}_{\text{model,NC}}^{ab}(\tilde{T}_{(1)}^{cd}, \tilde{T}_{(2)}^{cd}, \dots; \tilde{T}_{\text{NC}}^{cd}), \end{aligned} \quad (2.13)$$

because

$$\tilde{T}_{\text{NC}}^{ab} \neq \frac{\partial \tilde{x}^a}{\partial x^i} \frac{\partial \tilde{x}^b}{\partial x^j} T_{\text{NC}}^{ij}. \quad (2.14)$$

This means that if we use a non-covariant model for the Reynolds stress, the RANS simulation performed in the  $(\tilde{t}, \tilde{\mathbf{x}})$  system differs from that done in the  $(t, \mathbf{x})$  system (see also Ariki 2015a, 2017). Hamba (2006a) discussed the error emanating from the difference between the true value and the model of the anisotropy tensor under the Euclidean transformation. The same discussion can be made for the general coordinate transformation. The true Reynolds stress must form a tensor as depicted in (2.11). Consider the norm of the difference between the model and the true value of the Reynolds stress,  $E \equiv \|R_{\text{model}}^{ij} - R_{\text{true}}^{ij}\|$ . If the model is covariant, the error is independent of the frame; namely,

$$\begin{aligned} \tilde{E} &\equiv \|\tilde{R}_{\text{model}}^{ab} - \tilde{R}_{\text{true}}^{ab}\| = \tilde{g}_{ac} \tilde{g}_{bd} (\tilde{R}_{\text{model}}^{ab} - \tilde{R}_{\text{true}}^{ab}) (\tilde{R}_{\text{model}}^{cd} - \tilde{R}_{\text{true}}^{cd}) \\ &= \frac{\partial x^i}{\partial \tilde{x}^a} \frac{\partial x^\ell}{\partial \tilde{x}^c} g_{i\ell} \frac{\partial x^j}{\partial \tilde{x}^b} \frac{\partial x^m}{\partial \tilde{x}^d} g_{jm} \frac{\partial \tilde{x}^a}{\partial x^p} \frac{\partial \tilde{x}^b}{\partial x^q} (R_{\text{model}}^{pq} - R_{\text{true}}^{pq}) \frac{\partial \tilde{x}^c}{\partial x^r} \frac{\partial \tilde{x}^d}{\partial x^s} (R_{\text{model}}^{rs} - R_{\text{true}}^{rs}) \\ &= g_{i\ell} g_{jm} (R_{\text{model}}^{ij} - R_{\text{true}}^{ij}) (R_{\text{model}}^{\ell m} - R_{\text{true}}^{\ell m}) = \|R_{\text{model}}^{ij} - R_{\text{true}}^{ij}\| = E. \end{aligned} \quad (2.15)$$

In contrast, if the modelled Reynolds stress  $R_{\text{model,NC}}^{ij}$  is not covariant, the error yields  $\tilde{E} \neq E$  owing to (2.13) or (2.14). Therefore, if the model for the Reynolds stress is not covariant, the error depends on the choice of the computational frame. Similarly, other scalar values,

e.g. the production of the turbulent kinetic energy, will be frame-dependent if we employ a non-covariant model for the Reynolds stress. Problems also arise when comparing the statistics in different coordinate systems using the non-covariant model. Let us consider the case that the  $(t, \mathbf{x})$  system is a computational frame, whereas the  $(\tilde{t}, \tilde{\mathbf{x}})$  system is following the curvature of the boundary. The Reynolds normal stress in the direction following the curvature of the boundary, say the  $\tilde{x}^\alpha$  direction, is calculated via

$$\tilde{R}^{\alpha\alpha}(\tilde{t}, \tilde{\mathbf{x}}) = \frac{\partial \tilde{x}^\alpha}{\partial x^i} \frac{\partial \tilde{x}^\alpha}{\partial x^j} R^{ij}(t, \mathbf{x}), \quad (2.16)$$

where the summation is not taken for  $\alpha$ . However, if we employ a non-covariant model for the Reynolds stress  $R_{\text{model,NC}}^{ij}$ , the transformation (2.16) does not provide the true value even when  $R_{\text{model,NC}}^{ij}$  is exactly modelled in the computational frame; namely

$$\frac{\partial \tilde{x}^\alpha}{\partial x^i} \frac{\partial \tilde{x}^\alpha}{\partial x^j} R_{\text{model,NC}}^{ij}(t, \mathbf{x}) \neq \tilde{R}_{\text{true}}^{\alpha\alpha}(\tilde{t}, \tilde{\mathbf{x}}). \quad (2.17)$$

Therefore, the covariance of the Reynolds stress is important for understanding the physics of curved turbulent flows.

### 2.2.3. Velocity gradient

We often employ the mean strain and vorticity tensors as  $T_{(n)}^{ij}$  for turbulence modelling. Note that the covariant derivative of the velocity gradient does not form a tensor under the general coordinate transformation (Ariki 2015a):

$$\tilde{\nabla}_b \tilde{U}^a = \frac{\partial \tilde{x}^a}{\partial x^i} \frac{\partial x^j}{\partial \tilde{x}^b} \nabla_j U^i - \tilde{\Omega}^F a_b + \tilde{\Gamma}_{bc}^a \frac{\partial \tilde{x}^c}{\partial t}, \quad (2.18)$$

because the transformation rule of the Christoffel symbol reads (Landau & Lifshitz 1975; Frewer 2009; Ariki 2015a)

$$\tilde{\Gamma}_{bc}^a = \frac{\partial \tilde{x}^a}{\partial x^i} \frac{\partial x^j}{\partial \tilde{x}^b} \frac{\partial x^\ell}{\partial \tilde{x}^c} \Gamma_{j\ell}^i + \frac{\partial \tilde{x}^a}{\partial x^i} \frac{\partial^2 x^j}{\partial \tilde{x}^b \partial \tilde{x}^c}. \quad (2.19)$$

The general form of the mean strain rate and absolute vorticity tensors,  $S^{ij}$  and  $W^{Aij}$ , can be defined via the transformation of the mean velocity gradient from an inertial frame  $(t^I, \mathbf{x}^I)$  as (Ariki 2015a)

$$S_{ij} = \frac{1}{2}(\Sigma_{ij} + \Sigma_{ji}), \quad W_{ij}^A = \frac{1}{2}(\Sigma_{ij} - \Sigma_{ji}), \quad (2.20)$$

where

$$\Sigma_b^a = \frac{\partial x^a}{\partial x^I i} \frac{\partial x^{Ij}}{\partial x^b} \nabla_j^I U^{Ii}. \quad (2.21)$$

Hence, in the authors' understanding, we must set a reference coordinate, e.g. an inertial frame, to formulate a generally covariant tensor as the rotation rate  $\tilde{\Omega}^{Fi}_j$  in (2.8) is defined as the relative motion to the  $(t, \mathbf{x})$  system.

## 2.3. Covariance and weak-equilibrium assumption

### 2.3.1. Generalisation of conventional approach

To derive an ARSM, the weak-equilibrium assumption is often imposed (see e.g. Pope 2000; Durbin 2018); namely, (1.2) is assumed to be satisfied in a  $(\tilde{t}, \tilde{\mathbf{x}})$  system where the anisotropy

tensor is defined by

$$b^{ij} = \frac{R^i}{K} - \frac{2}{3}g^{ij}, \quad (2.22)$$

where  $K (= R^i/2)$  denotes the turbulent kinetic energy. For rotating or curved turbulent flows, the ARSM is constructed in a way that finds the frame  $(\tilde{t}, \tilde{\mathbf{x}})$ , which is not necessarily identical to the computational frame, that is assumed to satisfy the relation (1.2) (Girimaji 1997; Gatski & Jongen 2000; Wallin & Johansson 2002; Gatski & Wallin 2004). However, there is concern that this modelling breaks the covariance (see e.g. Weis & Hutter 2003). We demonstrate that the models obtained in this approach can be covariant. To discuss the covariance of the Reynolds stress, we write the transport equation for the anisotropy tensor using a covariant time derivative (see e.g. Thiffeault 2001). When we choose the convective or Oldroyd derivative along with the mean velocity (hereafter, mean Oldroyd derivative)  $\mathfrak{D}/\mathfrak{D}t$ , the transport equation for the anisotropy tensor can be written symbolically as (see e.g. Ariki 2015a, 2017)

$$\frac{\mathfrak{D}b^{ij}}{\mathfrak{D}t} = \left( \frac{\partial}{\partial t} + U^\ell \nabla_\ell \right) b^{ij} - (\nabla_\ell U^i) b^{\ell j} - (\nabla_\ell U^j) b^{i \ell} = f^{ij}(T_{(1)}^{\ell m}, T_{(2)}^{\ell m}, \dots). \quad (2.23)$$

Both the left and right-hand sides of (2.23) form tensors because the Oldroyd derivative of tensors also forms a tensor (Oldroyd 1950; Speziale 1987; Thiffeault 2001; Ariki 2015a, 2017). Hence, the anisotropy transport in the  $(\tilde{t}, \tilde{\mathbf{x}})$  system yields

$$\frac{\mathfrak{D}\tilde{b}^{ab}}{\mathfrak{D}\tilde{t}} - \tilde{f}^{ab}(\tilde{T}_{(1)}^{cd}, \tilde{T}_{(2)}^{cd}, \dots) = \frac{\partial \tilde{x}^a}{\partial x^i} \frac{\partial \tilde{x}^b}{\partial x^j} \left[ \frac{\mathfrak{D}b^{ij}}{\mathfrak{D}t} - f^{ij}(T_{(1)}^{\ell m}, T_{(2)}^{\ell m}, \dots) \right] = 0. \quad (2.24)$$

When the weak-equilibrium condition (1.2) is satisfied in the  $(\tilde{t}, \tilde{\mathbf{x}})$  system, the implicit relation for the anisotropy tensor yields

$$\tilde{U}^c (\tilde{\Gamma}_{dc}^a \tilde{b}^{db} + \tilde{\Gamma}_{dc}^b \tilde{b}^{ad}) - (\tilde{\nabla}_c \tilde{U}^a) \tilde{b}^{cb} - (\tilde{\nabla}_c \tilde{U}^b) \tilde{b}^{ac} = \tilde{f}^{ab}(\tilde{T}_{(1)}^{cd}, \tilde{T}_{(2)}^{cd}, \dots). \quad (2.25)$$

If we substitute some models into  $\tilde{f}^{ab}$  such as that proposed by Launder *et al.* (1975) and neglect diffusion terms, the resulting implicit ARSM equation yields

$$\tilde{b}^{ab} = -\tilde{C}_1 \tau \tilde{S}^{ab} - \tilde{C}_2 \tau [\tilde{S}_c^a \tilde{b}^{cb} + \tilde{S}_c^b \tilde{b}^{ca}]_{\text{tl}} - \tilde{C}_3 \tau [(\tilde{W}^{Aa}_c + \tilde{Y}^a_c) \tilde{b}^{cb} + (\tilde{W}^{Ab}_c + \tilde{Y}^b_c) \tilde{b}^{ca}], \quad (2.26)$$

where  $\tau$  is the turbulent time scale usually expressed by the turbulent kinetic energy and its dissipation rate,

$$\tilde{Y}^a_b = \tilde{\Gamma}^a_{bc} \tilde{U}^c - \tilde{\nabla}_b \tilde{U}^a, \quad (2.27)$$

and  $[A^{ij}]_{\text{tl}} (= A^{ij} - A^\ell_\ell g^{ij}/3)$  depicts the traceless part of  $A^{ij}$ .  $\tilde{C}_1$ ,  $\tilde{C}_2$ , and  $\tilde{C}_3$  are constant parameters. For rotating or curved turbulent flows, we construct an ARSM in the  $(\tilde{t}, \tilde{\mathbf{x}})$  system by assuming (1.2) and then transform it into the computational frame, say  $(t, \mathbf{x})$  (Girimaji 1997; Gatski & Jongen 2000; Wallin & Johansson 2002; Gatski & Wallin 2004). Following this strategy, the implicit ARSM in the computational frame  $(t, \mathbf{x})$  yields

$$b^{ij} = -\tilde{C}_1 \tau S^{ij} - \tilde{C}_2 \tau [S_\ell^i b^{\ell j} + S_\ell^j b^{\ell i}]_{\text{tl}} - \tilde{C}_3 \tau [(W^{Ai}_\ell + Y^{Ri}_\ell) b^{\ell j} + (W^{Aj}_\ell + Y^{Rj}_\ell) b^{\ell i}], \quad (2.28)$$

where

$$Y^{Ri}_j = \frac{\partial x^i}{\partial \tilde{x}^a} \frac{\partial \tilde{x}^b}{\partial x^j} \tilde{Y}^a_b. \quad (2.29)$$



Here,  $\tilde{Y}_b^a$  in (2.27) does not form a tensor in the sense that

$$\tilde{Y}_b^a \neq \frac{\partial x^i}{\partial \tilde{x}^a} \frac{\partial \tilde{x}^b}{\partial x^j} Y_j^i, \quad Y_j^i = \Gamma_{j\ell}^i U^\ell - \nabla_j U^i. \quad (2.30)$$

In contrast, we can confirm that  $Y_j^{Ri}$  in (2.29) forms a tensor. If we consider an additional coordinate frame  $(t^*, \mathbf{x}^*)$ , we have

$$Y_q^{R*p} = \frac{\partial x^{*p}}{\partial x^i} \frac{\partial x^j}{\partial x^{*q}} Y_j^{Ri} = \frac{\partial x^{*p}}{\partial x^i} \frac{\partial x^j}{\partial x^{*q}} \frac{\partial x^i}{\partial \tilde{x}^a} \frac{\partial \tilde{x}^b}{\partial x^j} \tilde{Y}_b^{Ra} = \frac{\partial x^{*p}}{\partial \tilde{x}^a} \frac{\partial \tilde{x}^b}{\partial x^{*q}} \tilde{Y}_b^{Ra}, \quad (2.31)$$

where  $\tilde{Y}_b^{Ra} = \tilde{Y}_b^a$ . Therefore,  $Y_q^{R*p}$  in the  $(t^*, \mathbf{x}^*)$  system is obtained via the transformation rule of tensor (1.1) both from the  $(t, \mathbf{x})$  system  $Y_j^{Ri}$  and the  $(\tilde{t}, \tilde{\mathbf{x}})$  system  $\tilde{Y}_b^{Ra}$ . Hamba (2006a) proposed the same discussion for the covariant property of the rotation rate in the Euclidean transformation. The definition of (2.29) is similar to the covariant velocity gradient (2.21) in the sense that it requires a reference frame.

### 2.3.2. Present approach using time derivative

As discussed in §2.3.1, the choice of the coordinate system where the weak-equilibrium assumption holds is essential for the development of ARSMs in rotating or curved turbulent flows (Girimaji 1997; Gatski & Jongen 2000; Wallin & Johansson 2002; Gatski & Wallin 2004). The mean acceleration (Girimaji 1997) and the eigenvectors of the mean strain rate (Gatski & Jongen 2000; Wallin & Johansson 2002) have been suggested as a coordinate system that is expected to satisfy the weak-equilibrium condition. The accuracy of the model depends on how to determine the coordinate system of reference. However, their assessment has not yet been completed (Brethouwer 2022). Furthermore, we cannot find the coordinate system in which the weak-equilibrium assumption holds for the periodically sheared turbulent flows as mentioned in the introduction (Yu & Girimaji 2006; Hamlington & Dahm 2008; Ariki & Ikeda 2023). Therefore, we consider an alternative modelling approach that does not rely on the choice of the frame. To develop generally covariant ARSMs, we adopt an approach that explicitly employs the time derivative of tensor quantities, as discussed in several studies (Yoshizawa 1984; Speziale 1987; Ahmadi & Chowdhury 1991; Taulbee 1992; Hamba 2006b; Hamlington & Dahm 2008; Ariki 2019; Ariki & Ikeda 2023). The Lagrangian derivative of the strain rate is also utilised as a scalar measure of flow curvature effects (Spalart & Shur 1997). In this study, we discuss the representation of the curvature effects by considering a covariant time derivative.

### 2.4. Basic equations for TC flow in featureless UR

For the TC flow, the ensemble average equals the average over the azimuthal direction and time. For the featureless UR, the turbulent field is also homogeneous in the axial direction. Thus, the mean velocity yields

$$\mathbf{U} = (U_r, U_\theta, U_z) = (0, U_\theta(r), 0). \quad (2.32)$$

Hereafter, we consider the homogeneity of turbulent fields in both the azimuthal and axial directions. Therefore, the RANS equation for the azimuthal velocity yields

$$-\frac{1}{r^2} \frac{d}{dr} (r^2 R_{r\theta}) + \nu \frac{1}{r^2} \frac{d}{dr} \left[ r^3 \frac{d}{dr} \left( \frac{U_\theta}{r} \right) \right] = 0. \quad (2.33)$$

The boundary conditions at the inner and outer cylinders are

$$\begin{aligned} U_\theta(r = r_{\text{in}}) &= r_{\text{in}}\omega_{\text{in}} = U_{\text{in}}, & U_\theta(r = r_{\text{out}}) &= r_{\text{out}}\omega_{\text{out}} = U_{\text{out}}, \\ R_{r\theta}(r = r_{\text{in}}) &= R_{r\theta}(r = r_{\text{out}}) = 0, \end{aligned} \quad (2.34)$$

where  $\omega_{\text{in}}$  and  $\omega_{\text{out}}$  denote the angular velocities of the inner and outer cylinders, respectively. In addition,  $r_{\text{in}}$  and  $r_{\text{out}}$  are the radii of the inner and outer cylinders, respectively. The parameters characterising the TC flow are the Reynolds number based on the inner-cylinder velocity and gap width  $Re_{\text{in}}$ , radius ratio  $\eta$ , and angular velocity ratio  $a$ , which are defined as

$$Re_{\text{in}} = \frac{U_{\text{in}}d}{\nu}, \quad \eta = \frac{r_{\text{in}}}{r_{\text{out}}}, \quad a = -\frac{\omega_{\text{out}}}{\omega_{\text{in}}}. \quad (2.35)$$

The flow regime of TC flows is often classified by the Taylor number  $Ta$ , which is defined as

$$Ta = \frac{(1 + \eta)^6}{64\eta^4} (1 + a)^2 Re_{\text{in}}^2. \quad (2.36)$$

The details of the derivation and physical meaning of this Taylor number are provided by Eckhardt *et al.* (2007). The UR of the TC turbulence is realised for the high- $Ta$  regime:  $Ta \gtrsim 10^9$  (Grossmann *et al.* 2016).

Integrating (2.33) from the inner cylinder to  $r$  provides a mean shear stress balance:

$$-r^2 R_{r\theta} + \nu r^3 \frac{d}{dr} \left( \frac{U_\theta}{r} \right) + r_{\text{in}}^2 u_\tau^2 = 0, \quad (2.37)$$

where  $u_\tau [= \sqrt{-\nu r d/dr(U_\theta/r)|_{r=r_{\text{in}}}}]$  denotes the friction velocity. In the bulk region, the viscous term decreases; thus, the mean shear stress balance yields

$$\frac{R_{r\theta}}{u_\tau^2} \simeq \left( \frac{r}{r_{\text{in}}} \right)^{-2}, \quad (2.38)$$

regardless of the outer cylinder rotation. Therefore, the Reynolds shear stress must be finite, even in a turbulent TC flow with outer cylinder rotation. The mean shear stress balance (2.37) also holds for the RANS simulations; thus, the asymptote in the bulk region (2.38) holds regardless of the model expression of the Reynolds stress at high Reynolds numbers.

### 2.5. Reynolds stress transport equations for TC turbulence

For the featureless UR of the TC turbulence, the transport equations for the Reynolds stress with nonzero production terms in the inertial frame are

$$\frac{DR_{rr}}{Dt} = -\frac{2U_\theta R_{r\theta}}{r} = P_{rr} - \varepsilon_{rr} + \Phi_{rr} + D_{rr}, \quad (2.39a)$$

$$\frac{DR_{\theta\theta}}{Dt} = \frac{2U_\theta R_{r\theta}}{r} = P_{\theta\theta} - \varepsilon_{\theta\theta} + \Phi_{\theta\theta} + D_{\theta\theta}, \quad (2.39b)$$

$$\frac{DR_{r\theta}}{Dt} = \frac{U_\theta(R_{rr} - R_{\theta\theta})}{r} = P_{r\theta} - \varepsilon_{r\theta} + \Phi_{r\theta} + D_{r\theta}, \quad (2.39c)$$

where  $D/Dt (= \partial/\partial t + U^i \nabla_i)$  denotes the Lagrangian or material time derivative along with mean velocity. Note that we define the Lagrangian derivative using the covariant derivative

$\nabla_i$ . The terms on the right-hand side are defined in the inertial frame as follows:

$$P^{ij} = -R_{i\ell} \nabla_\ell U^j - R^{j\ell} \nabla_\ell U^i, \quad (2.40a)$$

$$\varepsilon^{ij} = 2\nu g^{\ell m} \langle (\nabla_\ell u'^i) (\nabla_m u'^j) \rangle, \quad (2.40b)$$

$$\Phi^{ij} = 2 \langle p' s^{ij'} \rangle, \quad (2.40c)$$

$$D^{ij} = -\nabla_\ell \langle u'^i u'^j u'^\ell \rangle + \langle p' u'^i \rangle g^{j\ell} + \langle p' u'^j \rangle g^{i\ell} - \nu g^{\ell m} \nabla_m R^{ij}. \quad (2.40d)$$

They are referred to as the production, dissipation, pressure–strain correlation, and total diffusion terms, respectively. The strain rate  $s_{ij}$  in the inertial frame is defined as

$$s_{ij} = \frac{1}{2} (\nabla_j u_i + \nabla_i u_j), \quad (2.41)$$

and  $s^{ij} = g^{i\ell} g^{jm} s_{\ell m}$ . Owing to the curvature, the production term for the wall-normal stress component  $P_{rr}$  is nonzero. Namely, the production terms yield

$$P_{rr} = -2R_{r\theta} \nabla_\theta U_r = 2R_{r\theta} \frac{U_\theta}{r}, \quad (2.42a)$$

$$P_{\theta\theta} = -2R_{\theta r} \nabla_r U_\theta = -2R_{r\theta} \frac{dU_\theta}{dr}, \quad (2.42b)$$

$$P_{r\theta} = -R_{rr} \nabla_r U_\theta - R_{\theta\theta} \nabla_\theta U_r = -R_{rr} \frac{dU_\theta}{dr} + R_{\theta\theta} \frac{U_\theta}{r}. \quad (2.42c)$$

### 2.6. Curvature effects in ARSM and weak-equilibrium assumption

For TC flows, we can also discuss the flow in a rotating frame, for example, rotating at the same angular velocity as that of the outer cylinder. Let the rotating frame be written as  $(t^\dagger, r^\dagger, \theta^\dagger, z^\dagger)$ , where the angular velocity with respect to an inertial frame is constant and its axis is in the  $z$  direction:  $\mathbf{\Omega} = (0, 0, \Omega_z^F)$  which satisfies  $\Omega_z^{F\dagger} = -\epsilon_{ij3} \Omega^{F\dagger ij} / 2 = \Omega_z^F$  in this transformation. Here,  $\epsilon^{ij\ell}$  denotes the permutation tensor in three dimensions. The transformations of the coordinates and velocity fields between the rotating and inertial frames respectively yield

$$\begin{aligned} t^\dagger &= t, \quad r^\dagger = r, \quad \theta^\dagger = \theta - \Omega_z^F t, \quad z^\dagger = z, \\ u_r^\dagger &= u_r, \quad u_\theta^\dagger = u_\theta - r\Omega_z^F, \quad u_z^\dagger = u_z. \end{aligned} \quad (2.43)$$

Therefore, the Reynolds stress is invariant under this transformation:

$$R_{ij}^\dagger = \langle u_i^\dagger u_j^\dagger \rangle = \langle u'_i u'_j \rangle = R_{ij}, \quad (2.44)$$

because  $U_\theta^\dagger = U_\theta - r\Omega_z^F$  and thus  $u_i^\dagger = u'_i$ . Notably, any ARSM must satisfy (2.44).

### 2.7. Constant mean angular momentum and zero mean absolute vorticity

In turbulent TC flows, the mean velocity profile in the bulk region is often approximated by a nearly constant mean angular momentum  $rU_\theta \simeq \text{const}$ . (Smith & Townsend 1982; Lewis & Swinney 1999; Froitzheim *et al.* 2017; Ezeta *et al.* 2018; Dong 2007; Brauckmann & Eckhardt 2013; Brauckmann *et al.* 2016; Froitzheim *et al.* 2019; Cheng *et al.* 2020; Deguchi 2023). A nearly constant mean angular momentum has also been observed in curved turbulent channel flows with strong curvature (Wattendorf 1935; Nagata & Kasagi 2004; Brethouwer 2022). Brauckmann *et al.* (2016) and Brethouwer (2022) discussed the relationship between the constant mean angular momentum and zero mean absolute vorticity in rotating turbulent shear flows because both correspond to neutral stability. A nearly zero mean absolute vorticity

state has been widely observed in the bulk region of turbulent channel or plane Couette flows (Johnston *et al.* 1972; Tanaka *et al.* 2000; Hamba 2006*b*; Grundestam *et al.* 2008; Xia *et al.* 2016; Kawata & Alfredsson 2016*a,b*).

Here, we show that the constant mean angular momentum in circular flows corresponds exactly to zero mean absolute vorticity. Absolute vorticity is the covariant form of vorticity in a rotating frame. For example, for orthogonal transformation from an inertial frame  $(t, \mathbf{x})$  to a rotating frame  $(t^\dagger, \mathbf{x}^\dagger)$  with a constant angular velocity  $\Omega^{\text{F}\dagger i} = -\epsilon^{ij\ell} \Omega_{j\ell}^{\text{F}\dagger} / 2$ , the vorticity tensor obeys the following transformation rule in the Euclidean coordinate systems (Weis & Hutter 2003; Gatski & Wallin 2004; Hamba 2006*a*; Ariki 2015*a*):

$$w^{\text{A}\dagger ab} = w^{\dagger ab} + \Omega^{\text{F}\dagger ab} = \frac{\partial x^{\dagger a}}{\partial x^i} \frac{\partial x^{\dagger b}}{\partial x^j} w^{ij}, \quad (2.45)$$

where  $w^{\text{A}\dagger ij}$  denotes the absolute vorticity tensor. In addition,  $w^{ij}$  and  $w^{\dagger ij}$  represent the vorticity matrices in the inertial and rotating frames, respectively, and are defined as

$$w_{ij} = \frac{1}{2} (\nabla_j u_i - \nabla_i u_j), \quad w^{\dagger}_{ij} = \frac{1}{2} (\nabla^{\dagger}_j u^{\dagger}_i - \nabla^{\dagger}_i u^{\dagger}_j), \quad (2.46)$$

with  $w^{ij} = g^{i\ell} g^{jm} w_{\ell m}$  and  $w^{\dagger ij} = g^{\dagger i\ell} g^{\dagger jm} w^{\dagger}_{\ell m}$ . Therefore, the zero mean absolute vorticity in the rotating frame  $W^{\text{A}\dagger ij} = \langle w^{\text{A}\dagger ij} \rangle = 0$  coincides with the zero mean vorticity in the inertial frame  $W^{ij} = \langle w^{ij} \rangle = 0$ . For a cylindrical coordinate with (2.32), the zero mean vorticity yields

$$W_{r\theta} = \frac{1}{2} \left( -\frac{U_\theta}{r} - \frac{dU_\theta}{dr} \right) = -\frac{1}{2r} \frac{d}{dr} (rU_\theta) = 0 \iff rU_\theta = \mathcal{L} = \text{const.}, \quad (2.47)$$

which represents the constant mean angular momentum.

Predicting the nearly zero mean absolute vorticity is a good benchmark for RANS models because it cannot be reproduced by standard linear eddy-viscosity models (Wallin & Johansson 2000, 2002; Gatski & Wallin 2004; Hamba 2006*b*). Therefore, the prediction of nearly constant angular momentum can also be a benchmark for constructing turbulence models for curved flows.

### 2.8. Implicit algebraic model accompanied by flow curvature effects

To verify the effect of flow curvature on the Reynolds stress in TC flows, we derive a model expression based on the Reynolds stress transport equations (2.39*a*)–(2.39*c*). According to primitive modelling by Pope (1975), we also assume that the total diffusion term (2.40*d*) is negligible. In addition, we use the model for dissipation (2.40*b*) and pressure–strain correlation (2.40*c*) proposed by Launder *et al.* (1975); namely, they are modelled in the inertial frame as

$$\varepsilon^{ij} = \frac{2}{3} \varepsilon g^{ij}, \quad (2.48a)$$

$$\Phi^{ij} = -C_S \varepsilon b^{ij} + C_{R1} K S^{ij} + C_{R2} K \left[ S^i_\ell b^{\ell j} + S^j_\ell b^{\ell i} \right]_{\text{ll}} + C_{R3} K \left( W^i_\ell b^{\ell j} + W^j_\ell b_{\ell i} \right), \quad (2.48b)$$

where  $C_S$ ,  $C_{R1}$ ,  $C_{R2}$ , and  $C_{R3}$  are the model constants. Note that we do not assume the weak-equilibrium condition, in contrast to Pope (1975). Under these conditions, the Reynolds stress

transport equations in the inertial frame yield

$$\begin{aligned} \frac{Db^{ij}}{Dt} = & - \left( C_S - 1 + \frac{P^K}{\varepsilon} \right) \frac{\varepsilon}{K} b^{ij} - \left( \frac{4}{3} - C_{R1} \right) S^{ij} \\ & - (1 - C_{R2}) \left[ S_\ell^i b^{\ell j} + S_\ell^j b^{\ell i} \right]_{\text{fl}} - (1 - C_{R3}) \left( W_\ell^i b^{\ell j} + W_\ell^j b^{\ell i} \right), \end{aligned} \quad (2.49)$$

where  $P^K (= P_i^i)$  denotes the production rate of the turbulent kinetic energy. For the featureless UR of the TC turbulence, the leading components of the Reynolds stress yield the following matrix equation:

$$\begin{aligned} & \begin{bmatrix} \frac{\varepsilon}{gK} & 0 & \frac{2}{3}C_2S_{r\theta} + 2C_3W_{r\theta} - \frac{2U_\theta}{r} \\ 0 & \frac{\varepsilon}{gK} & \frac{2}{3}C_2S_{r\theta} - 2C_3W_{r\theta} + \frac{2U_\theta}{r} \\ C_2S_{r\theta} - C_3W_{r\theta} + \frac{U_\theta}{r} & C_2S_{r\theta} + C_3W_{r\theta} - \frac{U_\theta}{r} & \frac{\varepsilon}{gK} \end{bmatrix} \begin{bmatrix} b_{rr} \\ b_{\theta\theta} \\ b_{r\theta} \end{bmatrix} \\ & = -2C_1K \begin{bmatrix} 0 \\ 0 \\ S_{r\theta} \end{bmatrix}, \end{aligned} \quad (2.50)$$

where

$$C_1 = \frac{2}{3} - \frac{C_{R1}}{2}, \quad C_2 = 1 - C_{R2}, \quad C_3 = 1 - C_{R3}, \quad g = \left( C_S - 1 + \frac{P^K}{\varepsilon} \right)^{-1}. \quad (2.51)$$

Thus, the solution for shear stress yields

$$R_{r\theta} (= K b_{r\theta}) = - \frac{2C_1}{1 + 4(g\tau)^2 [-C_2^2 S_{r\theta}^2 / 3 + (C_3 W_{r\theta} - U_\theta / r)^2]} g \tau K S_{r\theta}, \quad (2.52)$$

where  $\tau = K/\varepsilon$ . In this expression,  $U_\theta/r$  in the denominator represents the effect of flow curvature on the Reynolds shear stress. This form of the model is essentially the same as that proposed by Wallin & Johansson (2000) for the two-dimensional case with its extension to the curved flows (Wallin & Johansson 2002). Strictly speaking, we should consider the  $S^{ij}$  dependence of  $P^K$  to derive a fully explicit ARSM (Girimaji 1996). We do not consider such sophistication to verify the effect of the flow curvature  $U_\theta/r$  on the Reynolds stress through the denominator. This representation of curvature effects is similar to the history effect in a swirling flow in a straight pipe proposed by Hamba (2017). They are essentially the same because they originate from the Lagrangian derivative of the Reynolds stress. In several ARSMs, the  $S_{r\theta}^2$  part in the denominator of (2.52) is often neglected because  $C_3 > C_2 = 1 - C_{R2} \approx 0$  is suggested by second-order or Reynolds stress transport models (e.g. Taulbee 1992; Wallin & Johansson 2000). In this study, we first verify the performance of the model based on (2.52) to extract the essence of representing the curvature effects. We address the construction of a covariant expression for curvature effects using a covariant time derivative in §4.

### 3. Verification of RANS model compared with experiments

In this section, we compare the performances of ARSMs with the experimental results to confirm which term significantly contributes to the Reynolds stress in the budget.

---

$a$	$Re_{\text{in}}$	$Re_{\text{out}}$	$Ta$
-0.5	$8.5 \times 10^4$	$5.8 \times 10^4$	$2.7 \times 10^9$
-0.33	$4.1 \times 10^4$	$1.9 \times 10^4$	$1.1 \times 10^9$
-0.33	$6.2 \times 10^4$	$2.8 \times 10^4$	$2.5 \times 10^9$
-0.33	$8.5 \times 10^4$	$3.9 \times 10^4$	$4.7 \times 10^9$
-0.1	$8.5 \times 10^4$	$1.2 \times 10^4$	$8.6 \times 10^9$
0	$4.1 \times 10^4$	0	$2.4 \times 10^9$
0	$6.2 \times 10^4$	0	$5.6 \times 10^9$
0	$8.5 \times 10^4$	0	$1.1 \times 10^{10}$
0.1	$8.5 \times 10^4$	$-1.2 \times 10^4$	$1.3 \times 10^{10}$

---

Table 1: Control parameters examined by the present experimental facility with  $\eta = 0.732$  and  $\Gamma = 18$ .  $Re_{\text{out}}$  is the outer cylinder Reynolds number:  $Re_{\text{out}} = U_{\text{out}}d/\nu$ .

---

### 3.1. Experimental setup

We utilised a very large facility to realise high-Reynolds-number TC turbulence. As its details are described in Horimoto & Okuyama (2025), we briefly explain our experimental setup here. The TC facility consists of an aluminum inner and an acrylic outer cylinder whose radii are  $r_{\text{in}} = 150$  mm and  $r_{\text{out}} = 205$  mm, respectively. The height of the annulus region between these cylinders is  $L = 990$  mm. Thus, the dimensionless geometric parameters in the present experiments are the radius ratio of  $\eta = 0.732$  and the aspect ratio of  $\Gamma = L/d = 18$ . The angular velocities of the two cylinders,  $\omega_{\text{in}}$  and  $\omega_{\text{out}}$ , are independently controlled by two stepper motors. The working fluid was degassed water. The examined parameter regimes are  $Re_{\text{in}} = O(10^4)$  and  $-0.5 \leq a \leq 0.1$ , which result in a  $Ta$  regime of  $O(10^9)$ – $O(10^{10})$ , as shown in table 1. Note that the present setup achieves a sufficiently high  $Ta$  for the UR:  $Ta \gtrsim O(10^9)$  (see also Grossmann *et al.* 2016).

We measured the turbulent velocity field in the  $r$ – $\theta$  plane at half-height of the gap by particle tracking velocimetry (PTV). In the present PTV, we used a house-made code with the following algorithm. In an instantaneous frame, we detected the positions of individual tracer particles and set a small interrogation region around each particle. By employing a direct cross-correlation method, we detected the particle positions in the next frame and calculated the displacement of particles. We removed error vectors with a threshold based on the first and third quantiles of the two-dimensional vector components,  $u_\theta$  and  $u_r$ , and finally obtained about 5000 velocity vectors in each frame. Here, note that these vectors were not spatially regular. Therefore, the gap width was divided into 100 thin annular regions with a constant width  $d/100$ , and the mean velocity  $U_\theta(r)$  was calculated by averaging the obtained velocity vectors over the azimuthal and time directions in each annulus. The dimensionless measurement time was at least  $8.1T$ , where  $T$  denotes the time scale of the bulk flow:  $T = d/(U_{\text{in}} - U_{\text{out}})$ .

### 3.2. Numerical setup

We performed the  $K$ – $\varepsilon$  RANS model. The baseline model is the conventional linear eddy-viscosity model proposed by Abe *et al.* (1994), which allows us to use the no-slip condition owing to the damping functions for wall-bounded flows. The governing equations are the RANS equation for the mean azimuthal velocity (2.33) and transport equations for the

turbulent kinetic energy  $K$  and its dissipation rate  $\varepsilon$ :

$$\frac{DK}{Dt} = -R_{r\theta}S_{r\theta} - \varepsilon + \frac{1}{r} \frac{d}{dr} \left[ r \left( \frac{\nu_T}{\sigma_K} + \nu \right) \frac{dK}{dr} \right] = 0, \quad (3.1)$$

$$\frac{D\varepsilon}{Dt} = -C_{\varepsilon 1} \frac{\varepsilon}{K} R_{r\theta}S_{r\theta} - C_{\varepsilon 2} f_{\varepsilon} \frac{\varepsilon^2}{K} + \frac{1}{r} \frac{d}{dr} \left[ r \left( \frac{\nu_T}{\sigma_{\varepsilon}} + \nu \right) \frac{d\varepsilon}{dr} \right] = 0, \quad (3.2)$$

where  $\nu_T$  is the eddy viscosity, which is defined as

$$\nu_T = C_{\nu} f_{\nu} \frac{K^2}{\varepsilon}. \quad (3.3)$$

$f_{\nu}$  and  $f_{\varepsilon}$  are damping functions defined as

$$f_{\nu} = \left\{ 1 - \exp \left[ -\frac{y}{a_1 \eta} \right] \right\}^2 \left\{ 1 + \frac{a_2}{Re_T^{3/4}} \exp \left[ -\left( \frac{Re_T}{a_3} \right)^2 \right] \right\}, \quad (3.4)$$

$$f_{\varepsilon} = \left\{ 1 - \exp \left[ -\frac{y}{a_{\varepsilon 1} \eta} \right] \right\}^2 \left\{ 1 - a_{\varepsilon 2} \exp \left[ -\left( \frac{Re_T}{a_{\varepsilon 3}} \right)^2 \right] \right\}, \quad (3.5)$$

where  $y$ ,  $\eta [= (\nu^3/\varepsilon)^{1/4}]$ , and  $Re_T [= K^2/(\nu\varepsilon)]$  denote the distance from the nearest wall, Kolmogorov length scale, and turbulent Reynolds number, respectively. Note again that we consider the featureless UR; thus, the statistics depend only on the radial position  $r$ . The model parameters were set as follows:

$$\begin{aligned} C_{\nu} &= 0.09, \quad C_{\varepsilon 1} = 1.5, \quad C_{\varepsilon 2} = 1.9, \quad \sigma_K = 1.4, \quad \sigma_{\varepsilon} = 1.4, \\ a_1 &= 14, \quad a_2 = 5, \quad a_3 = 200, \quad a_{\varepsilon 1} = 3.1, \quad a_{\varepsilon 2} = 0.3, \quad a_{\varepsilon 3} = 6.5. \end{aligned} \quad (3.6)$$

The velocity and length were normalised by the inner-cylinder velocity  $U_{in} (= r_{in}\omega_{in})$  and gap width between the cylinders  $d$ . The boundary conditions were (2.34) and

$$\begin{aligned} K(r = r_{in}) &= K(r = r_{out}) = 0, \\ \varepsilon(r = r_{in}) &= \nu \frac{1}{r} \frac{d}{dr} \left( r \frac{dK}{dr} \right) (r = r_{in}), \quad \varepsilon(r = r_{out}) = \nu \frac{1}{r} \frac{d}{dr} \left( r \frac{dK}{dr} \right) (r = r_{out}). \end{aligned} \quad (3.7)$$

For the original linear eddy-viscosity model proposed by Abe *et al.* (1994), the Reynolds shear stress is given by

$$R_{r\theta} = -2\nu_T S_{r\theta}. \quad (3.8)$$

Hereafter, we refer to the model using Eqs. (2.33), (3.1), (3.2), (3.3), and (3.8) as the AKN model. To observe the effect of the flow curvature, we employed the following algebraic model of the Reynolds shear stress according to (2.52):

$$R_{r\theta} = -\frac{2C_1}{1 + 4\tau_T^2(C_3 W_{r\theta} - C_r U_{\theta}/r)^2} \tau_T K S_{r\theta}, \quad \tau_T = C_{\tau} f_{\nu} \frac{K}{\varepsilon}. \quad (3.9)$$

We refer to this model as the curvature-corrected ARSM (ccARSM) because this model is essentially the same as that proposed by Wallin & Johansson (2002).  $C_{\tau}$  corresponds to  $C_5^{-1}$  for the production–dissipation equilibrium condition  $P^K/\varepsilon = 1$ . Compared with (2.52), we removed the  $S_{r\theta}^2$  term from the denominator for the ccARSM, as is often assumed in several ARSMs (e.g. Taulbee 1992; Wallin & Johansson 2000). We also examined the model with the strain rate in the denominator and confirmed that it was ineffective in predicting TC flows (see Appendix C). Note that  $C_r$ , which is unity in (2.52), is an artificially introduced

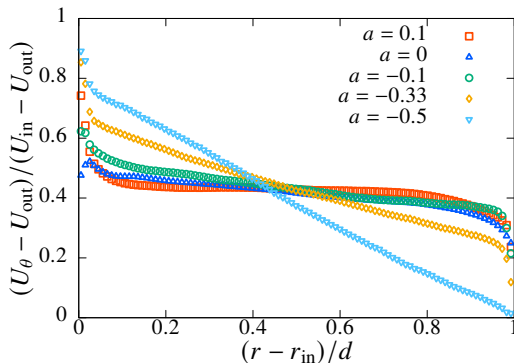


Figure 1: Mean velocity profiles of experiments for various angular velocity ratios  $a$  at  $Re_{in} = 8.5 \times 10^4$ .

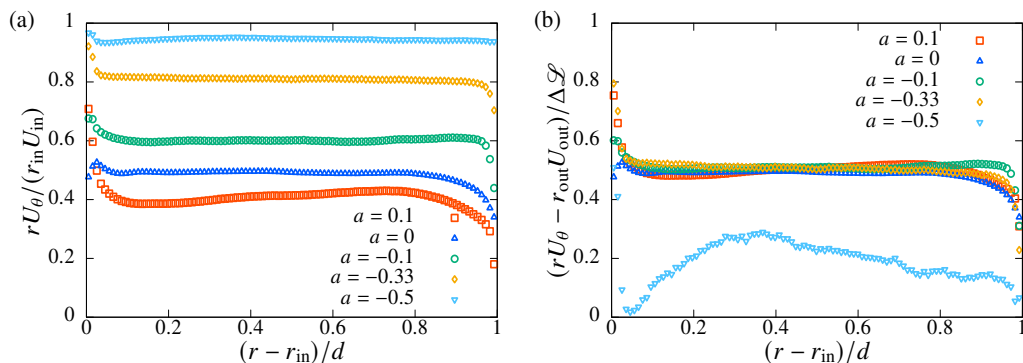


Figure 2: Mean angular momentum profiles of the experiments for various  $a$  at  $Re_{in} = 8.5 \times 10^4$  normalised by (a) the angular momentum of the inner cylinder and (b) the angular momentum difference between the inner and outer cylinders.

parameter to examine the curvature effect through  $U_\theta/r$ . In other words, the curvature effect can be switched off by setting  $C_r = 0$ , which corresponds to the standard ARSM proposed by Pope (1975) although the strain rate was removed from the denominator of the Reynolds shear stress. Hereafter, we fixed  $C_1 = C_v/C_\tau$  such that the ccARSM yields the AKN model when  $C_3 = C_r = 0$ . In addition, we fixed  $C_\tau = 1/3.9$  so that the ccARSM provides a good prediction for various flow parameters. In this study, we focus on the existence of the contributions of  $W_{r\theta}$  or  $U_\theta/r$  in the denominator to the Reynolds stress; therefore, we set  $C_3$  and  $C_r$  to 0 or 1.

### 3.3. Results

#### 3.3.1. Experimental results

Figure 1 depicts the mean velocity profiles in the experiments for various angular velocity ratios  $a$ . The mean velocity is normalised such that it yields values of 1 and 0 at the inner and outer cylinders, respectively. In this normalisation, the gradient of the mean velocity becomes steeper as  $a$  decreases. The TC flow is Rayleigh stable for  $r_{in}^2 \omega_{in} < r_{out}^2 \omega_{out}$  or  $-a > \eta^2$  for  $\omega_{in} > 0$  (Rayleigh 1917). For our experimental apparatus, the critical line is  $a = -0.536$ . Therefore,  $a = -0.5$  is close to the stability line; thus, the mean velocity profile looks similar to the laminar profile.

Figure 2(a) depicts the mean angular momentum profiles normalised by the angular



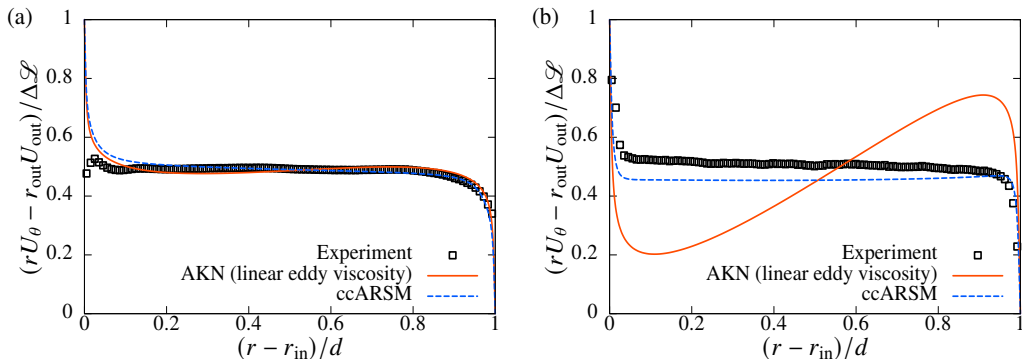


Figure 3: Mean angular momentum profiles of AKN and ccARSM compared with those of experiments at  $Re_{in} = 8.5 \times 10^4$  for (a)  $a = 0$  and (b)  $a = -0.33$ .

momentum of the inner cylinder. The nearly constant angular momentum seems universal in the bulk region  $0.1 < (r - r_{in})/d < 0.9$  for  $a < 0.1$ . In this normalisation, the constant value of the angular momentum increases as  $a$  decreases. This trend is natural because the angular momentum will be bounded by  $-a/\eta^2 \leq rU_\theta/(r_{in}U_{in}) \leq 1$  if its profile is almost monotonic. For  $a = 0.1$ , the angular momentum exhibits a shallow positive gradient. This may be caused by the Taylor rolls. To verify this, we must perform averaging over different heights in the future.

Brauckmann *et al.* (2016) numerically showed that the mean angular momentum profiles collapse to 0.5 in a bulk region for weakly counter-rotating and co-rotating cases when they are normalised by the angular momentum difference between the inner and outer cylinders and adjusted to 1 and 0 at the inner and outer cylinders, respectively. Figure 2(b) depicts the mean angular momentum profiles normalised by the angular momentum difference between the inner and outer cylinders:  $\Delta\mathcal{L} = r_{in}U_{in} - r_{out}U_{out} = r_{in}^2\omega_{in} - r_{out}^2\omega_{out}$ . In addition, they are adjusted to 1 and 0 at the inner and outer cylinders, respectively. Our results also collapse to 0.5 except for  $a = -0.5$ . For our apparatus,  $a = -0.5$  is close to the Rayleigh stable line:  $a = -\eta^2 = -0.536$ . When  $a$  is close to the Rayleigh stable line, the denominator  $\Delta\mathcal{L}$  becomes small; thus, the result is much more susceptible to errors. Furthermore, the flow may no longer be in the UR owing to the stabilisation effect. The outlier for  $a = -0.5$  may be caused by this flow property or by related difficulties in velocimetry.

### 3.3.2. Performance of ccARSM

Figure 3 depicts the mean angular momentum profiles of the RANS models compared with the experiments at  $Re_{in} = 8.5 \times 10^4$ . Hereafter, we adopt the normalisation by the angular momentum difference between the inner and outer cylinders. As seen in Fig. 3(a), both the AKN (linear eddy-viscosity) model and ccARSM predict the mean angular momentum for  $a = 0$ . However, figure 3(b) shows that the AKN model fails to predict the nearly constant mean angular momentum for  $a = -0.33$ . Therefore, the conventional linear eddy-viscosity model is irrelevant for predicting TC flows. In contrast, the ccARSM fairly succeeds in predicting a nearly constant mean angular momentum for both  $a = 0$  and  $a = -0.33$ . The emergence of a nearly constant mean angular momentum is independent of the Reynolds and Taylor numbers for both experiments and ccARSM for  $Ta \gtrsim O(10^9)$  (see Appendix B).

Figure 4 depicts the mean angular momentum for several sets of model parameters of ccARSM for  $a = -0.33$ . When the curvature effect is removed by setting  $C_r = 0$ , the model fails to predict an experimental profile, similarly to the AKN model for  $a = -0.33$  depicted in figure 3(b). In contrast, even when we set  $C_3 = 0$ , the ccARSM fairly reproduced the nearly

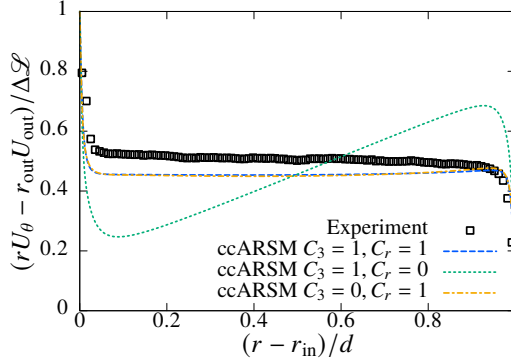


Figure 4: Mean angular momentum profiles for several sets of model parameters of ccARSM for  $a = -0.5$  at  $Re_{in} = 8.5 \times 10^4$ .

constant mean angular momentum, as same as the case of  $C_3 = C_r = 1$ . Therefore, we can conclude that the  $U_\theta/r$ -related part in the denominator of (3.9) is essential for expressing the curvature effects in TC flows. The difference between the present ccARSM and that proposed by Wallin & Johansson (2002) is only the value of constant parameters and near-wall treatments. We infer that the explicit ARSM proposed by Wallin & Johansson (2002) also predicts the nearly constant mean angular momentum as it has the essence,  $U_\theta/r$ -related part. The fine-tuning of constant parameters is out of the scope of this study.

## 4. Discussion

### 4.1. Construction of covariant ARSM accompanied by flow curvature effects

The nearly constant mean angular momentum can be predicted using the conventional ARSMs accompanied by the curvature effects (Girimaji 1997; Gatski & Jongen 2000; Wallin & Johansson 2002; Gatski & Wallin 2004) because the direction of the mean flow is obvious. This study aims to develop an alternative model expression that represents the flow curvature effects without assuming the mean flow direction. We adopt covariant time derivatives to express the flow curvature effects as an extension of the models employing the time derivative terms (Yoshizawa 1984; Speziale 1987; Ahmadi & Chowdhury 1991; Taulbee 1992; Hamba 2006b; Hamlington & Dahm 2008; Ariki 2019; Ariki & Ikeda 2023).

Ariki (2017) discussed the covariance of ARSM in a cylindrical coordinate based on the time integration of the mean strain rate with a relaxation time expressed by the turbulence time scale. They demonstrated that the integration of the mean strain rate along the Lagrangian derivative is not covariant, whereas that along the upper-convected or Oldroyd derivative yields a covariant linear eddy-viscosity model. However, the latter does not incorporate the correction due to the flow curvature; that is, the  $U_\theta/r$  term in the denominator of (2.52) does not appear. Therefore, it does not predict the nearly constant mean angular momentum observed in the TC flows. To construct a covariant ARSM accompanied by flow curvature effects, we employ the Jaumann derivative as an alternative candidate for the covariant time derivative. Specifically, we employ the Jaumann derivative along with the mean velocity, which is hereafter referred to as the mean Jaumann derivative. The mean Jaumann derivative of a second-rank contravariant tensor is defined in an inertial frame as follows (see e.g. Oldroyd 1958; Goddard & Miller 1966; Thiffeault 2001):

$$\frac{\mathcal{D}A^{ij}}{\mathcal{D}t} = \frac{DA^{ij}}{Dt} - W^i_\ell A^{\ell j} - W^j_\ell A^{i\ell}. \quad (4.1)$$

The expression in a general coordinate system is given in Appendix D. The modelled transport equation for the anisotropy tensor (2.49) can be rewritten via the mean Jaumann derivative as

$$\begin{aligned} \frac{\mathcal{D}b^{ij}}{\mathcal{D}t} = & - \left( C_S - 1 + \frac{PK}{\varepsilon} \right) \frac{\varepsilon}{K} b^{ij} - \left( \frac{4}{3} - C_{R1} \right) S^{ij} \\ & - (1 - C_{R2}) \left[ S_{\ell}^i b^{\ell j} + S_{\ell}^j b^{\ell i} \right]_{\text{tl}} - (2 - C_{R3}) \left( W^{Ai}_{\ell} b^{\ell j} + W^{Aj}_{\ell} b^{\ell i} \right). \end{aligned} \quad (4.2)$$

According to previous ARSMs (Taulbee 1992; Wallin & Johansson 2000) and our results, setting  $C_{R2} = 1$  is physically acceptable. Thus, the transport equation is reduced to

$$\frac{\mathcal{D}b^{ij}}{\mathcal{D}t} = - \left( C_S - 1 + \frac{PK}{\varepsilon} \right) \frac{\varepsilon}{K} b^{ij} - \left( \frac{4}{3} - C_{R1} \right) S^{ij} - (2 - C_{R3}) \left( W^{Ai}_{\ell} b^{\ell j} + W^{Aj}_{\ell} b^{\ell i} \right). \quad (4.3)$$

If we adopt the mean Oldroyd derivative instead of the Jaumann derivative, the transport equation for the anisotropy tensor yields (see also Ariki 2015a, 2017)

$$\begin{aligned} \frac{\mathfrak{D}b^{ij}}{\mathfrak{D}t} = & - \left( C_S - 1 + \frac{PK}{\varepsilon} \right) \frac{\varepsilon}{K} b^{ij} - \left( \frac{4}{3} - C_{R1} \right) S^{ij} \\ & - (2 - C_{R2}) \left[ S_{\ell}^i b^{\ell j} + S_{\ell}^j b^{\ell i} \right]_{\text{tl}} - (2 - C_{R3}) \left( W^{Ai}_{\ell} b^{\ell j} + W^{Aj}_{\ell} b^{\ell i} \right). \end{aligned} \quad (4.4)$$

Compared with (4.2), the coefficient of the third term on the right-hand side yields  $2 - C_{R2}$ . Thus, the contribution of strain rates to the transport equation cannot be neglected as done in (4.3), even if we set  $C_{R2} = 1$ . To simplify the Reynolds stress transport while holding the covariance, employing the mean Jaumann derivative is better than doing the mean Oldroyd derivative.

To derive an ARSM that incorporates curvature effects, we consider the following normalisation:

$$\widehat{S}^{ij} = \frac{K}{\varepsilon} S^{ij}, \quad \widehat{W}^{Aij} = \frac{W^{Aij}}{\sqrt{W^{A\ell m} W_{\ell m}^A}}, \quad \lambda = \frac{K}{\varepsilon} \sqrt{W^{A\ell m} W_{\ell m}^A}, \quad \frac{\mathcal{D}}{\widehat{\mathcal{D}t}} = \frac{K}{\varepsilon} \frac{\mathcal{D}}{\mathcal{D}t}, \quad (4.5)$$

which leads to the following transport equation:

$$g^{-1} b^{ij} + \frac{\mathcal{D}b^{ij}}{\mathcal{D}t} = -2C_1 \widehat{S}^{ij} - C_{\mathcal{D}3} \lambda \left( \widehat{W}^{Ai}_{\ell} b^{\ell j} + \widehat{W}^{Aj}_{\ell} b^{\ell i} \right), \quad (4.6)$$

where  $g$  and  $C_1$  are defined in (2.51), and  $C_{\mathcal{D}3} = 2 - C_{R3} = 1 + C_3$ . For a nearly constant mean angular momentum in an inertial frame or zero mean absolute vorticity,  $\sqrt{W^{A\ell m} W_{\ell m}^A}$  is very small; thus,  $\lambda$  is a small parameter, whereas  $\widehat{W}^{Aij}$  can be finite. To incorporate the time-derivative effect, we expand the anisotropy tensor as follows:

$$b^{ij} = b_{(0)}^{ij} + \lambda b_{(1)}^{ij} + \dots \quad (4.7)$$

Up to  $O(\lambda)$ , we have

$$g^{-1} b_{(0)}^{ij} + \frac{\mathcal{D}b_{(0)}^{ij}}{\mathcal{D}t} = -2C_1 \widehat{S}^{ij}, \quad (4.8a)$$

$$g^{-1} b_{(1)}^{ij} + \frac{\mathcal{D}b_{(1)}^{ij}}{\mathcal{D}t} = -C_{\mathcal{D}3} \left( \widehat{W}^{Ai}_{\ell} b_{(0)}^{\ell j} + \widehat{W}^{Aj}_{\ell} b_{(0)}^{\ell i} \right). \quad (4.8b)$$

These equations can be formally solved as follows (Goddard & Miller 1966; Hamlington & Dahm 2008; Hamba 2017; Arika 2017):

$$b_{(0)}^{ij} = -2C_1 \int^{\hat{t}} \mathcal{D}\hat{t}' \exp \left[ - \int_{\hat{t}'}^{\hat{t}} \mathcal{D}\hat{t}'' g^{-1}|_{\hat{t}''} \right] \widehat{S}^{ij}|_{\hat{t}'}, \quad (4.9a)$$

$$b_{(1)}^{ij} = -C_{\mathcal{D}3} \int^{\hat{t}} \mathcal{D}\hat{t}' \exp \left[ - \int_{\hat{t}'}^{\hat{t}} \mathcal{D}\hat{t}'' g^{-1}|_{\hat{t}''} \right] \left( \widehat{W}^{Ai}{}_{\ell} b_{(0)}^{\ell j} + \widehat{W}^{Aj}{}_{\ell} b_{(0)}^{\ell i} \right) \Big|_{\hat{t}'}, \quad (4.9b)$$

where  $\int \mathcal{D}t$  denotes the time integration along the mean Jaumann transport and  $\cdot|_t$  denotes the time label along the transport path. The time-local expression is obtained by performing a derivative expansion of integrands (Hamlington & Dahm 2008):

$$A^{ij}|_{\hat{t}} = A^{ij}|_{\hat{t}'} - \frac{\mathcal{D}A^{ij}}{\mathcal{D}\hat{t}} \Big|_{\hat{t}'} (\hat{t} - \hat{t}') + \dots. \quad (4.10)$$

Consequently, up to  $O(\lambda)$  and the first time derivative, we obtain the following algebraic expression for the anisotropy tensor:

$$\begin{aligned} b^{ij} = & -2C_1 h_{(0)} \widehat{S}^{ij} + 2C_1 h_{(1)} \frac{\mathcal{D}\widehat{S}^{ij}}{\mathcal{D}\hat{t}} - 2C_1 C_{\mathcal{D}3} h_{(0)}^2 \lambda \left( \widehat{S}^i{}_{\ell} \widehat{W}^{A\ell j} + \widehat{S}^j{}_{\ell} \widehat{W}^{A\ell i} \right) \\ & + 2C_1 C_{\mathcal{D}3} h_{(0)} h_{(1)} \lambda \left( \frac{\mathcal{D}\widehat{S}^i{}_{\ell}}{\mathcal{D}\hat{t}} \widehat{W}^{A\ell j} + \frac{\mathcal{D}\widehat{S}^j{}_{\ell}}{\mathcal{D}\hat{t}} \widehat{W}^{A\ell i} \right) \\ & + 2C_1 C_{\mathcal{D}3} h_{(1)} \lambda \frac{\mathcal{D}}{\mathcal{D}\hat{t}} \left[ h_{(0)} \left( \widehat{S}^i{}_{\ell} \widehat{W}^{A\ell j} + \widehat{S}^j{}_{\ell} \widehat{W}^{A\ell i} \right) \right] + \dots, \end{aligned} \quad (4.11)$$

where

$$h_{(n)} = \frac{1}{n!} \int^{\hat{t}} \mathcal{D}\hat{t}' \exp \left[ - \int_{\hat{t}'}^{\hat{t}} \mathcal{D}\hat{t}'' g^{-1}|_{\hat{t}''} \right] (\hat{t} - \hat{t}')^n. \quad (4.12)$$

The expression (4.11) can also be derived via the iterative expansion of (4.2) (Hamba 2006b). For unsteady turbulent flows,  $h_{(n)}$  depends on time according to the histories of  $K/\varepsilon$  and  $g$ . The ARSM involving the time derivative of the strain rate, i.e. the second term of the first line of (4.11), has been discussed in several studies (Speziale 1987; Ahmadi & Chowdhury 1991; Taulbee 1992; Hamlington & Dahm 2008) and derived from statistical closure theories (Yoshizawa 1984; Arika 2019; Arika & Ikeda 2023). Spalart & Shur (1997) proposed a scalar measure of the curvature effects using the Lagrangian derivative of the strain rate. Hamba (2006b) employed the Lagrangian time derivative in a rotating frame of  $S_{\ell}^i W^{A\ell j} + S_{\ell}^j W^{A\ell i}$  to elucidate the occurrence of nearly zero mean absolute vorticity profiles in bulk of spanwise-rotating turbulent channel flows. Several studies have employed the upper-convected or Oldroyd time derivative to achieve a covariant expression of ARSM (Speziale 1987; Hamlington & Dahm 2008; Arika 2019; Arika & Ikeda 2023).

For a statistically two-dimensional flow with a circular mean velocity expressed by  $U_{\theta} = U_{\theta}(r)$  (2.32), the  $O(\lambda)$  terms in (4.11) have nonzero contributions to the shear stress. Under (2.32) in the inertial frame, we have

$$\frac{\mathcal{D}\widehat{S}^i{}_{\ell}}{\mathcal{D}\hat{t}} \widehat{W}^{\ell j} + \frac{\mathcal{D}\widehat{S}^j{}_{\ell}}{\mathcal{D}\hat{t}} \widehat{W}^{\ell i} = \frac{\mathcal{D}}{\mathcal{D}\hat{t}} (\widehat{S}^i{}_{\ell} \widehat{W}^{\ell j} + \widehat{S}^j{}_{\ell} \widehat{W}^{\ell i}). \quad (4.13)$$

Therefore, the shear component of the time-derivative term in (4.11) yields

$$\frac{\mathcal{D}S_{r\theta}}{\mathcal{D}t} = 0, \quad \frac{\mathcal{D}}{\mathcal{D}t}(S_{r\ell}W_{\ell\theta} + S_{\theta\ell}W_{\ell r}) = -4 \left( W_{r\theta} + \frac{U_\theta}{r} \right) W_{r\theta} S_{r\theta}, \quad (4.14)$$

in cylindrical coordinates in the inertial frame, where the latter is similar to the model proposed by Hamba (2006b); namely, they employed a term proportional to

$$\frac{D}{Dt}(S_{r\ell}W_{\ell\theta} + S_{\theta\ell}W_{\ell r}) = -4 \frac{U_\theta}{r} W_{r\theta} S_{r\theta}, \quad (4.15)$$

in an inertial frame. Notably, Hamba (2006b) succeeded in predicting the nearly zero mean absolute vorticity by employing (4.15) in a rotating frame. As discussed in §2.7, the zero mean absolute vorticity in a rotating frame corresponds to constant angular momentum in an inertial frame. In contrast,  $\mathcal{D}S_{r\theta}/\mathcal{D}t = 0$ . The essential part for predicting the nearly constant mean angular momentum is the  $U_\theta/r$ -related part in (4.14) as observed in §3.3.2, which is common to the model proposed by Hamba (2006b). When  $K$ ,  $\varepsilon$ , and  $g$  are constant along the mean streamline, we have  $h_{(n)} = g^{n+1}$ . Comparing (2.52) and (3.9), we may have  $g = C_\tau f_\nu = C_\nu f_\nu / C_1$ . Consequently, a simple covariant model expression expected to predict the nearly constant angular momentum in the inertial frame of TC flow will be as follows:

$$\begin{aligned} [R^{ij}]_{\text{II}} = & -2\nu_T S^{ij} + C_D \frac{\nu_T^2}{K} \frac{\mathcal{D}S^{ij}}{\mathcal{D}t} - C_Q \frac{\nu_T^2}{K} (S_\ell^j W^{\ell j} + S_\ell^j W^{\ell i}) \\ & + C_J f_\nu^2 \frac{K^2}{\varepsilon^2} \nu_T \frac{\mathcal{D}}{\mathcal{D}t} (S_\ell^i W^{\ell j} + S_\ell^j W^{\ell i}), \end{aligned} \quad (4.16)$$

where  $C_D = 2/C_1$ ,  $C_Q = 2C_{\mathcal{D}3}/C_1$ , and  $C_J = 4C_{\mathcal{D}3}C_\tau^2$  are constant parameters. Specifically, the shear stress can be written as

$$R_{r\theta} = -2\nu_T \left[ 1 + 2C_J f_\nu^2 \frac{K^2}{\varepsilon^2} \left( W_{r\theta} + \frac{U_\theta}{r} \right) W_{r\theta} \right] S_{r\theta}. \quad (4.17)$$

Hereafter, we refer to the model expressed by (4.16) or (4.17) as the Jaumann derivative model (JDM). The JDM is also reduced to the AKN model when  $C_J = 0$ .

#### 4.2. Verification of JDM

We verify the performance of the JDM in the TC flow. The numerical procedure is the same as that described in §3.2. Namely, we numerically solve Eqs. (2.33), (3.1), and (3.2) with (3.3) and (4.17). In the convergence calculation, we employ the following regularisation to avoid numerical divergence due to negative diffusion:

$$R_{r\theta} = -2\nu_T f_J S_{r\theta}, \quad f_J = \max \left[ 1 + 2C_J f_\nu^2 \frac{K^2}{\varepsilon^2} \left( W_{r\theta} + \frac{U_\theta}{r} \right) W_{r\theta}, 0.01 \right] \quad (4.18)$$

Note that we confirmed that the convergent results yielded  $f_J > 0.01$  for all cases (figure not shown).

Figure 5 depicts the model parameter  $C_J$  dependence of the JDM in predicting the mean angular momentum. As  $C_J$  increases, the profiles tend to become almost constant and are saturated at  $C_J = 1.2$ . Thus, the newly introduced Jaumann derivative term appropriately represents the curvature effects in the TC flow because it predicts a nearly constant mean angular momentum. Hereafter, we fix  $C_J = 1.2$ .

Figure 6 depicts the mean angular momentum profiles for several values of  $a$ . The profiles are nearly constant in the bulk region and collapse to approximately 0.5 for all the cases

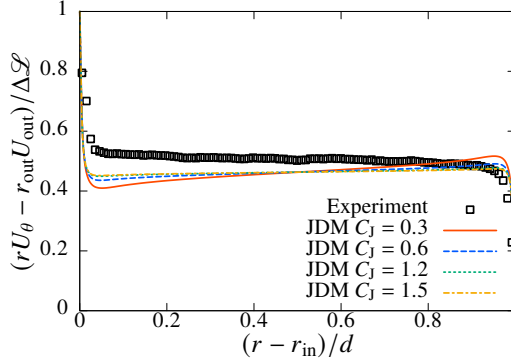


Figure 5: Model parameter  $C_J$  dependence of JDM at  $Re_{in} = 8.5 \times 10^4$  for  $a = -0.33$ .

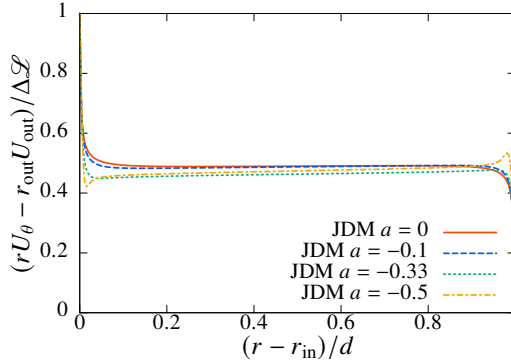


Figure 6: Angular momentum profiles of JDM compared with those of experiments at  $Re_{in} = 8.5 \times 10^4$  for  $a = 0, -0.1, -0.33,$  and  $-0.5$ .

including  $a = -0.5$ . Therefore, we expect that the JDM is an effective and simple model expression that represents the flow curvature effects.

### 4.3. Physical properties of JDM

#### 4.3.1. Comparison with cubic eddy-viscosity models

Flow curvature effects are often expressed using the cubic-eddy-viscosity model, e.g.  $S_\ell^i W_m^{A\ell} W^{Amj} + S_\ell^j W_m^{A\ell} W^{Ami}$ , in ARSMs. The form of this term is similar to that of the second term on the right-hand side of the JDM (4.16). However, their origins are slightly different. In the present parameter expansion on  $\lambda$  resulting in (4.9a) and (4.9b) with the derivative expansion (4.10), the JDM appears at  $O(\lambda)$  and first order of time derivative. According to the derivation of ARSM (see e.g. Pope 1975; Taulbee 1992; Yoshizawa 1998), the term like  $S_\ell^i W_m^{A\ell} W^{Amj} + S_\ell^j W_m^{A\ell} W^{Ami}$  appears at  $O(\lambda^2)$ . This is easily confirmed by neglecting the time-derivative term in the parameter expansion; in this case,  $b_{(n)}^{ij}$ 's up to

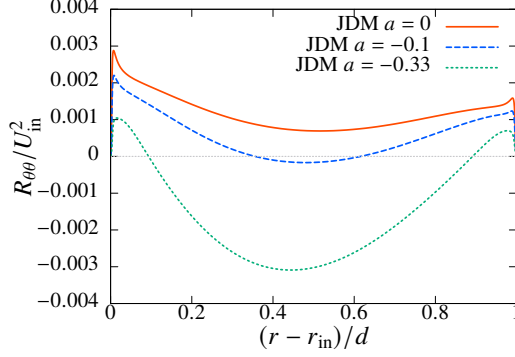


Figure 7: Profiles of the azimuthal component of the Reynolds normal stress  $R_{\theta\theta}$  of the JDM at  $Re_{in} = 8.5 \times 10^4$  for  $a = 0, -0.1, \text{ and } -0.33$ .

$O(\lambda^2)$  yield

$$b_{(0)}^{ij} = -2C_1 g \widehat{S}^{ij}, \quad (4.19a)$$

$$b_{(1)}^{ij} = -C_{\mathcal{Q}3} g (\widehat{W}^{Ai}{}_{\ell} b_{(0)}^{\ell j} + \widehat{W}^{Aj}{}_{\ell} b_{(0)}^{\ell i}) = 2C_1 C_{\mathcal{Q}3} g^2 (\widehat{W}^{Ai}{}_{\ell} \widehat{S}^{\ell j} + \widehat{W}^{Aj}{}_{\ell} \widehat{S}^{\ell i}), \quad (4.19b)$$

$$b_{(2)}^{ij} = -C_{\mathcal{Q}3} (\widehat{W}^{Ai}{}_{\ell} b_{(1)}^{\ell j} + \widehat{W}^{Aj}{}_{\ell} b_{(1)}^{\ell i}) = -2C_1 C_{\mathcal{Q}3}^2 g^3 (\widehat{W}^{Ai}{}_{\ell} \widehat{W}^{A\ell}{}_m \widehat{S}^{mj} + \widehat{W}^{Aj}{}_{\ell} \widehat{W}^{A\ell}{}_m \widehat{S}^{mi}). \quad (4.19c)$$

Furthermore, its contribution to the shear stress in cylindrical coordinates in the inertial frame also differs from that of the JDM because

$$b_{(2),r\theta} = 4C_1 C_{\mathcal{Q}3}^2 g^3 \widehat{W}_{r\theta}^2 \widehat{S}_{r\theta}. \quad (4.20)$$

Namely, the  $U_{\theta}/r$ -related part does not appear. This cubic model (4.20) effectively decreases the effects of eddy viscosity, which corresponds to the  $W_{r\theta}$  term in the denominator of ARSM (2.52) or (3.9) (see also Yoshizawa 1998; Yoshizawa *et al.* 2006), which was ineffective in predicting the nearly constant mean angular velocity in the featureless UR of the TC turbulence. This is consistent with the conventional understanding of the ARSM as the rotation effect emanating from the coordinate transformation of the Lagrangian derivative, which modifies the cubic-eddy-viscosity term obtained in an inertial frame, is essential for predicting the zero mean absolute vorticity (Wallin & Johansson 2002; Gatski & Wallin 2004; Hamba 2006b). Therefore, we can conclude that the effects of rotating or flow curvatures should be considered separately in addition to the conventional cubic-eddy-viscosity models. The JDM is a candidate for the expression in a generally covariant form.

#### 4.3.2. Reynolds normal stress

Quadratic statistics such as the turbulent kinetic energy or Reynolds normal stresses should be discussed to evaluate turbulence models. However, in our experiments, there were two difficulties in measuring the velocity fluctuations accurately. First, we could not set a dynamic range enough to resolve the velocity fluctuations. This is because there is a bottleneck due to a large difference in the magnitudes of  $u_{\theta}$  and  $u_r$  (recall that the mean radial velocity is  $U_r \approx 0$  for the co-rotating cases). Second, the velocity fluctuations become small as the flow condition approaches the Rayleigh stability criterion ( $a = -\eta^2 = -0.536$  in the present experiment) as mentioned in §3.3.1. We have confirmed that the mean velocity profiles are well-converged independent of the algorithm employed for the velocimetry. Here, we only discuss the qualitative properties of the JDM.

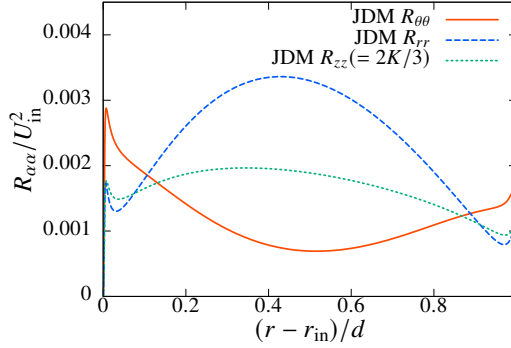


Figure 8: Profiles of the normal components of the Reynolds normal stress  $R_{\alpha\alpha}$  of the JDM at  $Re_{in} = 8.5 \times 10^4$  for  $a = 0$ .

The azimuthal component of the Reynolds normals stress for the JDM in the inertial frame yields

$$\begin{aligned} R_{\theta\theta} &= \frac{2}{3}K + C_D \frac{v_T^2}{K} \frac{\mathcal{D}S_{\theta\theta}}{\mathcal{D}t} - 2C_Q \frac{v_T^2}{K} S_{\theta\ell} W_{\ell\theta} \\ &= \frac{2}{3}K + 2C_D \frac{v_T^2}{K} \left( \frac{U_\theta}{r} + W_{r\theta} \right) S_{r\theta} - 2C_Q \frac{v_T^2}{K} W_{r\theta} S_{r\theta}. \end{aligned} \quad (4.21)$$

Following the result of parameter expansion and parameters employed for the ccARSM and JDM, we set  $C_D = 2/C_1$ ,  $C_Q = 2C_{\mathcal{D}3}/C_1 = C_J/(2C_\tau C_1)$  with  $C_1 = C_\nu/C_\tau$ ,  $C_\nu = 0.09$ ,  $C_\tau = 1/3.9$ , and  $C_J = 1.2$ . Figure 7 depicts the azimuthal component of the Reynolds normal stress of the JDM for several values of  $a$ . The value in the bulk region decreases as  $a$  decreases and becomes negative for  $a \leq -0.1$ . Hence, one of the reliability conditions Schumann (1977),  $R_{\alpha\alpha} \geq 0$ , is broken. The negative normal stress is caused by the second term of the right-hand side of (4.21), which emanates from the Jaumann derivative of the mean strain rate. The breakage of realisability is often observed for the simple models with constant coefficients (see e.g. Shih *et al.* 1993);  $C_\nu$  and  $C_J$  for the JDM. Further sophistication is required to develop realisable turbulence models (see e.g. Hanjalić & Launder 2011; Mishra & Girimaji 2014; Ariki 2015b; Inagaki *et al.* 2019; Ariki & Ikeda 2023). We do not perform such a fine-tuning in this study because it is out of the scope of the development of model expression for curvature effects. However, we will see that a relatively simple modification of the coefficients makes the JDM realisable later.

Although the JDM provides the negative normal stress, the trend that the value in the bulk region decreases as  $a$  decreases is plausible; the flow becomes stable as  $a$  approaches the Rayleigh stable line  $a = -\eta^2$ . This trend can be explained in terms of the Reynolds stress budget. In the transport equation for the azimuthal component of the Reynolds normal stress (2.39b),  $2U_\theta R_{r\theta}/r$  emanating from the convection term contributes to the budget as an additional production term, which is negative because  $U_\theta, R_{r\theta} > 0$ . The value of  $U_\theta$  increases as the outer cylinder rotation increases in the same direction as the inner cylinder. Hence, the negative contribution to the budget increases, resulting in the decrease of  $R_{\theta\theta}$ . The same trend was also observed in rotating or curved turbulent channel flows (Hamba 2006b; Brethouwer 2022). Therefore, we infer that the JDM qualitatively captures the physics of curved turbulent flows.

Ezeta *et al.* (2018) experimentally investigated the turbulence statistics of TC flows in the UR for  $a = 0$ . The radius ratio of their apparatus ( $\eta = 0.714$ ) and the range of  $Ta$  are comparable to our experiments. The root-mean-square (RMS) of the azimuthal component



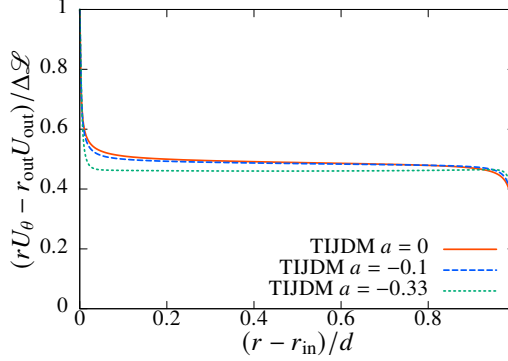


Figure 9: Angular momentum profiles of TIJDM compared with those of experiments at  $Re_{in} = 8.5 \times 10^4$  for  $a = 0, -0.1, \text{ and } -0.33$ .

of velocity fluctuation normalised by the inner cylinder velocity was approximately 0.03 for high  $Ta$  cases. They showed that the radial component of velocity fluctuation is slightly larger than that of the azimuthal component in the bulk region. Figure 8 depicts the profiles of the normal components of the Reynolds normal stress of the JDM for  $a = 0$ . Note that  $b_{rr} = -b_{\theta\theta}$  and  $b_{zz} = 0$ , and thus  $R_{rr} = 4K/3 - R_{\theta\theta}$  and  $R_{zz} = 2K/3$  for the JDM. The JDM qualitatively reproduces the trend of the magnitude of the azimuthal and radial components of velocity fluctuation. The value of the RMS of the azimuthal velocity fluctuation  $\sqrt{R_{\theta\theta}}/U_{in}$  is approximately 0.03 in the bulk region. The ratio of the RMS of the radial component to that of the azimuthal component approximately yields 2 in the bulk region, which is slightly larger than the value 1.5 observed by Ezeta *et al.* (2018). Therefore, these values are not far from the experimental results of the UR of TC flows for  $a = 0$ . We infer that the JDM has the potential to quantitatively predict the statistics of the UR of the TC flows by the fine-tuning of the model parameters.

#### 4.3.3. Analytical Jaumann integration for featureless UR

We obtained the JDM by truncating the derivative expansion at the first time derivative. For the featureless UR of the TC flow, we can analytically integrate (4.9a) and (4.9b) (see e.g. Goddard & Miller 1966; Hamlington & Dahm 2008; Hamba 2017; Ariki 2019). Alternatively, we can obtain the integrated form by performing the derivative expansion (4.10) and renormalise the expanded result via  $1/(1+x) = 1+x+x^2+\dots$ . We refer to the fully time-integrated Jaumann model as TIJDM. Consequently, the Reynolds shear stress in the inertial frame yields

$$R_{r\theta} = -\frac{2C_1}{1 + 4(g\tau)^2(W_{r\theta} + U_\theta/r)^2} \times \left[ 1 + \frac{8C_{\mathcal{D}3}}{1 + 4(g\tau)^2(W_{r\theta} + U_\theta/r)^2} (g\tau)^2 \left( W_{r\theta} + \frac{U_\theta}{r} \right) W_{r\theta} \right] g\tau K S_{r\theta}. \quad (4.22)$$

Figure 9 depicts the mean angular momentum profiles of the TIJDM for several values of  $a$ . The profiles are almost constant in the bulk region and similar to those of the JDM depicted in figure 6. Compared with (4.17), an additional correction  $(g\tau)^2(W_{r\theta} + U_\theta/r)^2$  appears in the denominator. Note that  $W_{r\theta} + U_\theta/r = -S_{r\theta}$ ; thus, this correction is the same as that using the strain rate discussed in Appendix C. Therefore, this correction is ineffective in predicting the constant mean angular momentum. This is the physical reason why the truncation of the first-order time derivative does not decrease the performance of the model in predicting the constant mean angular momentum.

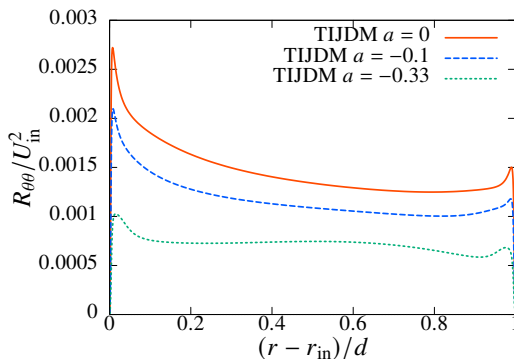


Figure 10: Profiles of the azimuthal component of the Reynolds normal stress  $R_{\theta\theta}$  of the TIJDM at  $Re_{in} = 8.5 \times 10^4$  for  $a = 0, -0.1, \text{ and } -0.33$ .

In contrast, the profiles of the Reynolds normal stress are changed. The time integration of the azimuthal component of the Reynolds normal stress in the inertial frame yields

$$R_{\theta\theta} = \frac{2}{3}K + 2C_D \frac{1}{1 + 4\tau_T^2(W_{r\theta} + U_\theta/r)^2} \frac{v_T^2}{K} \left( W_{r\theta} + \frac{U_\theta}{r} \right) S_{r\theta} - 2C_Q \frac{1 - 4(g\tau)^2(W_{r\theta} + U_\theta/r)^2}{[1 + 4(g\tau)^2(W_{r\theta} + U_\theta/r)^2]^2} \frac{v_T^2}{K} S_{r\theta} W_{r\theta}, \quad (4.23)$$

Figure 10 depicts the profiles of the azimuthal component of the Reynolds normal stress of the TIJDM for several values of  $a$ . The problem of the negative normal stress observed in the JDM depicted in figure 7 is resolved. Note that time integration is not a unique solution to the breakage of realisability. The correction in the denominator of the second term of (4.23) can be written by  $S_{r\theta}$  as stated in the preceding paragraph. Time integration is impractical when employing the algebraic type of Reynolds stress models. An important finding is that the realisable expression can be developed for ARSMs employing the time derivative terms.

#### 4.3.4. Physical property of JDM in other curved or rotating turbulent flows

For spanwise rotating channel flows, the Reynolds shear stress of JDM in a rotating frame ( $t^\dagger, \mathbf{x}^\dagger$ ) yields

$$R_{xy}^\dagger = -2\nu_T S_{xy}^\dagger - 4C_J f_v^2 \frac{K^2}{\varepsilon^2} \nu_T W_{xy}^\dagger W_{xy}^{A\dagger} S_{xy}^\dagger. \quad (4.24)$$

When the mean absolute vorticity is nearly zero, we may approximate  $W_{xy}^\dagger W_{xy}^{A\dagger} = (W_{xy}^{A\dagger} + \Omega_z^F) W_{xy}^{A\dagger} \simeq \Omega_z^F W_{xy}^{A\dagger}$  because  $\Omega_z^F \gg W_{xy}^{A\dagger}$ , indicating that (4.24) is essentially the same as the model proposed by Hamba (2006b), which succeeds in predicting the nearly zero mean absolute vorticity in spanwise rotating turbulent channel flows. Thus, the JDM can also predict a nearly zero mean absolute vorticity in spanwise rotating turbulent channel flows. Spalart & Shur (1997) proposed a scalar measure of curvature effects using the Lagrangian derivative of the strain rate, namely  $2W^{ij}S_{j\ell}DS_\ell^i/Dt$  in the inertial frame. Hamba (2006b) discussed that the model term of the time derivative of  $S_\ell^i W^{A\ell j} + S_\ell^j W^{A\ell i}$  can also be a three-dimensional expression of curvature effects. Hamba (2006b) validated the relevance of incorporating the time-derivative term in terms of the Reynolds stress budget. Because the JDM can be considered as a covariant extension of the model proposed by Hamba (2006b), our model is a candidate for a more general expression of flow curvature effects in complex turbulent flows.

The essence of the curvature effects in the JDM or ccARSM originates from the convection term. For curved channel flows, Brethouwer (2022) showed that additional production owing to the convection term becomes prominent in the streamwise and wall-normal components of the Reynolds stress as the curvature increases. Abe (2019) suggested that the convection of the Reynolds shear stress has a large value around the separating bubble. In this separating flow, the anisotropy tensor seems to vary along the streamline. Therefore, expressing the curvature effects using the convection term is physically relevant. We expect that modelling the curvature effects using time-derivative terms will improve the prediction of other curved or rotating turbulent flows.

#### 4.3.5. Comparison with the model using Oldroyd derivative

Although we employed the Jaumann derivative for convenience in deriving the model, covariant ARSMs can be constructed using other covariant time derivatives. For example, if we rewrite the JDM (4.16) using the mean Oldroyd derivative, we may have

$$\begin{aligned} [R^{ij}]_{\text{tl}} = & -2\nu_{\text{T}}S^{ij} + C_{\text{DO}}\frac{\nu_{\text{T}}^2}{K}\frac{\mathfrak{D}S^{ij}}{\mathfrak{D}t} - C_{\text{QO}}\frac{\nu_{\text{T}}^2}{K}(S_{\ell}^iW^{\text{Al}j} + S_{\ell}^jW^{\text{Al}i}) \\ & + C_{\text{O}}f_{\text{v}}^2\frac{K^2}{\varepsilon^2}\nu_{\text{T}}\frac{\mathfrak{D}}{\mathfrak{D}t}(S_{\ell}^iW^{\text{Al}j} + S_{\ell}^jW^{\text{Al}i}), \end{aligned} \quad (4.25)$$

where  $C_{\text{OD}}$ ,  $C_{\text{OQ}}$ , and  $C_{\text{O}}$  are constant parameters. The second term on the right-hand side of (4.25) has already been proposed previously (Speziale 1987; Hamlington & Dahm 2008; Ariki 2019; Ariki & Ikeda 2023). In cylindrical coordinates in the inertial frame, the mean Oldroyd (upper-convected) derivative of  $S_{r\ell}W_{\ell\theta} + S_{\theta\ell}W_{\ell r}$  yields

$$\frac{\mathfrak{D}}{\mathfrak{D}t}(S_{r\ell}W_{\ell\theta} + S_{\theta\ell}W_{\ell r}) = 2\left(\frac{\partial U_{\theta}}{\partial r} - \frac{U_{\theta}}{r}\right)W_{r\theta}S_{r\theta} = -4\left(W_{r\theta} + \frac{U_{\theta}}{r}\right)W_{r\theta}S_{r\theta}, \quad (4.26)$$

which is identical to the latter of (4.14). This can be confirmed by calculating the difference between two derivatives in the inertial frame according to (D 5):

$$\begin{aligned} & \frac{\mathfrak{D}}{\mathfrak{D}t}(S_{r\ell}W_{\ell\theta} + S_{\theta\ell}W_{\ell r}) - \frac{\mathfrak{D}}{\mathfrak{D}t}(S_{r\ell}W_{\ell\theta} + S_{\theta\ell}W_{\ell r}) \\ & = S_{rm}(S_{m\ell}W_{\ell\theta} + S_{\theta\ell}W_{\ell m}) + S_{\theta m}(S_{r\ell}W_{\ell m} + S_{m\ell}W_{\ell r}) = 0, \end{aligned} \quad (4.27)$$

in the featureless UR of the TC flow. Therefore, for the TC flows, the difference between the Jaumann and Oldroyd derivatives is inapparent at the low-order terms. However, the model expressions are different for the higher-order terms, e.g. time-integration of the mean strain rate. When considering the steady state with the mean velocity  $\mathbf{U} = (U_r, U_{\theta}, U_z) = (0, U_{\theta}(r), 0)$  similar to the featureless UR of the TC turbulence, the Jaumann integral of the shear component of the mean strain rate corresponding to (4.9a) yields

$$\int_{-\infty}^t \mathfrak{D}t' \exp\left[-\frac{\varepsilon}{gk}(t-t')\right] S_{r\theta}|_{t'} = \frac{gK/\varepsilon}{1+4(gK/\varepsilon)^2(W_{r\theta} + U_{\theta}/r)^2} S_{r\theta}. \quad (4.28)$$

This result corresponds to the first part of (4.22). In contrast, the similar integral along with the Oldroyd derivative yields (Ariki 2017)

$$\int_{-\infty}^t \mathfrak{D}t' \exp\left[-\frac{\varepsilon}{gk}(t-t')\right] S_{r\theta}|_{t'} = \frac{gK}{\varepsilon} S_{r\theta}. \quad (4.29)$$

Therefore, the performance of these models can be different when considering the higher-order time derivative terms. To observe the detailed difference, we may have to evaluate the

models in more complex turbulent flows such as three-dimensional shear flows. This is one of the future works.

#### 4.4. Generalisation of ARSM

Although we have expanded the model up to  $O(\lambda)$ , a general model expression requires much more tensor bases. We must evaluate the performance of the model accompanied by the Jaumann derivative terms in more complex curved turbulent flows in future. To do this, the generalisation of the model must be discussed. Pope (1975) suggested that the Reynolds stress is expressed via the ten bases when the model is expanded using the velocity gradient. The number of bases increases significantly if we employ additional bases involving the covariant time derivative. Namely, the examples of additional bases are as follows:

$$\frac{\mathcal{D}S^{ij}}{\mathcal{D}t}, \frac{\mathcal{D}}{\mathcal{D}t}(S_\ell^i W^{A\ell j} + S_\ell^j W^{A\ell i}), \frac{\mathcal{D}}{\mathcal{D}t}(S_\ell^i W^{A\ell}_m W^{Amj} + S_\ell^j W^{A\ell}_m W^{Ami}), \frac{\mathcal{D}^2 S^{ij}}{\mathcal{D}t^2}, \dots \quad (4.30)$$

Wallin & Johansson (2000) suggested that the two-dimensional expression of ARSM, which includes up to the quadratic term on the velocity gradient, performs well for several basic turbulent flows. The exception is the three-dimensional flow such as the turbulence in an axially rotating pipe (e.g. Imao *et al.* 1996; Orlandi & Fatica 1997). Practically, up to the cubic models have been employed even for three-dimensional turbulent flows (e.g. Craft *et al.* 1996; Speziale *et al.* 2000; Wallin & Johansson 2000). The higher-order time-derivative terms may be impractical. Then, a practical expression based on the present parameter expansion (4.7) with (4.3) will yield

$$\begin{aligned} R^{ij} = & \frac{2}{3} K g^{ij} - 2F_{(1)} \tau S^{ij} - F_{(2)} \tau^2 (S_\ell^i W^{A\ell j} + S_\ell^j W^{A\ell i}) + F_{(3)} \tau^2 [S_\ell^i S^{\ell j}]_{\text{u}} \\ & + F_{(4)} \tau^3 \left[ S_\ell^i W^{A\ell}_m W^{Amj} + S_\ell^j W^{A\ell}_m W^{Ami} \right]_{\text{u}} \\ & + F_{(5)} \tau^2 \frac{\mathcal{D}S^{ij}}{\mathcal{D}t} + F_{(6)} \tau^3 \frac{\mathcal{D}}{\mathcal{D}t} (S_\ell^i W^{A\ell j} + S_\ell^j W^{A\ell i}), \end{aligned} \quad (4.31)$$

where  $F_{(n)}$ 's are non-dimensional coefficients and  $\tau = K/\varepsilon$  for the  $K-\varepsilon$  models ( $\tau = \omega^{-1}$  for the  $K-\omega$  models). Note that the  $S_\ell^i S^{\ell j}$  term is artificially added; it does not appear if the parameter expansion is performed in (4.3). However, this term is essential for reproducing the redistribution of energies between the streamwise and spanwise components in the wall-bounded parallel shear flows. The additional term  $S_\ell^i S_\ell^m W^{Amj} + S_\ell^j S_\ell^m W^{Ami}$  may be needed to increase the accuracy of the model.  $F_{(n)}$ 's are expressed using the invariants, e.g.  $II_S = S^{ij} S_{ij}$ ,  $II_W = W^{Aij} W^A_{ji}$ ,  $III_S = S_j^i S_\ell^j S_\ell^i$ , or  $I_{SWW} = S_j^i W^{Aj}_\ell W^{A\ell}_i$ . In addition, we have new invariants such as

$$II_{\mathcal{D}S} = \frac{\mathcal{D}S^{ij}}{\mathcal{D}t} \frac{\mathcal{D}S_{ij}}{\mathcal{D}t}, \quad II_{\mathcal{D}SW} = \frac{\mathcal{D}}{\mathcal{D}t} (S_\ell^i W^{A\ell j} + S_\ell^j W^{A\ell i}) \frac{\mathcal{D}}{\mathcal{D}t} (S_{im} W^{Am}_j + S_{jm} W^{Am}_i). \quad (4.32)$$

We can additionally employ the third invariants of the strain rates or the time derivative terms. For the wall-bounded turbulent flows, the near-wall treatment is also essential. It is almost impossible to sophisticate the coefficients  $F_{(n)}$  by hand. However, data-driven modelling allows us to find the best combination of the invariants with constant parameters. We believe that the general covariance of the model increases the reliability and accuracy of the data-augmented turbulence models.

## 5. Conclusions

A generally covariant Reynolds-averaged Navier–Stokes (RANS) model using covariant time derivatives was proposed for predicting rotating and curved turbulent flows. We showed that the conventional ARSM accompanied by the rotation or flow curvature effects (Girimaji 1997; Gatski & Jongen 2000; Wallin & Johansson 2002; Gatski & Wallin 2004) can be covariant if a curvilinear coordinate system is properly determined as a reference frame, which is the extension of the discussion by Hamba (2006a) to a general coordinate transformation. Our model using the covariant time derivative has the advantage of not needing to find a reference frame where the weak-equilibrium assumption (1.2) holds.

We evaluated the performance of RANS models in the featureless ultimate regime (UR) of Taylor–Couette (TC) turbulence, in which the statistics are one-dimensional in the radial direction. Prediction of the nearly constant mean angular momentum observed in the UR of TC turbulence was considered as a benchmark. To verify the physical origin of the effect of the curvature on the Reynolds stress in TC flows, we examined the curvature-corrected algebraic Reynolds stress model (ccARSM) by incorporating the convection effect in the Reynolds stress budgets. The performance of the ccARSM was verified by comparing it with high-Reynolds-number TC experiments with independently rotating cylinders. The experimental results showed universal profiles of a nearly constant mean angular momentum in the bulk region, mainly for the co-rotating cases, which is consistent with the numerical results of Brauckmann *et al.* (2016). For the RANS simulation, the conventional linear eddy-viscosity model did not predict the nearly constant mean angular momentum for the co-rotating case although it worked fairly well for the case in which only the inner cylinder rotated. In contrast, the ccARSM predicts the mean angular momentum profiles well for both cases. Parameter analysis of the ccARSM showed that the curvature effect emanating from the convection of the Reynolds stress is essential for predicting the nearly constant angular momentum for the co-rotating case.

To develop ARSMs that incorporate the curvature effect emanating from the convection term, we introduced the Jaumann derivative as a covariant time derivative (Oldroyd 1958; Goddard & Miller 1966; Thiffeault 2001; Frewer 2009). The small parameter expansion according to the nearly constant angular momentum led to the ARSM employing time-derivative terms, which is referred to as the Jaumann derivative model (JDM) in this study. The JDM also succeeded in predicting nearly constant angular momentum profiles for a wide range of co-rotating turbulent TC flows, including the case in which only the inner cylinder rotates. The JDM is covariant under any coordinate transformation. The essence of the curvature effects in the JDM is the time-derivative term emanating from the convection of the Reynolds stress. The convection of the Reynolds stress becomes prominent in several curved or rotating turbulent flows (e.g. Hamba 2006b; Abe 2019; Brethouwer 2022). The JDM becomes unrealisable in the sense that the normal stress yields negative when the outer-cylinder rotation increases. However, the trend of the value of the azimuthal component of the Reynolds normal stress against the outer cylinder rotation was consistent with other rotating or curved turbulent flows (Hamba 2006b; Brethouwer 2022). The ratio of the velocity fluctuation of the radial component to that of the azimuthal component was reasonable for  $a = 0$  compared with the experiments by Ezeta *et al.* (2018). We provided an extension of the ARSM by adding the Jaumann derivative terms. Although the form of the model is complex, a data-driven or machine-learning approach will make it possible to determine the model coefficients with several invariants. We believe that the generally covariant property of the model improves the accuracy of the data-driven or machine-learning models, as the previous studies incorporating mathematical constraints improved the accuracy (Ling *et al.* 2016; Wu *et al.* 2018; Duraisamy *et al.* 2019; Jiang *et al.* 2021; Horie & Mitsume 2024).

**Acknowledgements.** The authors acknowledge Prof. Hiromichi Kobayashi at Keio University for valuable discussions and Mr. Homare Okuyama for his experimental support. The authors are grateful to the anonymous referees for their valuable comments on the improvement of this paper.

**Funding.** K. I. was supported by Grant-in-Aid for JSPS Fellows Grant No. JP22KJ2660 and Grant-in-Aid from the Harris Science Research Institute of Doshisha University. Y. H. was supported by JSPS KAKENHI (C) Grant No. JP22K03917.

**Declaration of interests.** The authors report no conflict of interest.

**Data availability statement.** The data that support the findings of this study are available from the corresponding author on reasonable request.

**Author ORCIDs.** K. Inagaki <https://orcid.org/0000-0002-9092-0526>; Y. Horimoto <https://orcid.org/0000-0002-1792-1282>

## Appendix A. Covariant form of spatial gradient in cylindrical coordinate

We write the velocity field in cylindrical coordinates as follows:

$$\mathbf{u} = u_r \mathbf{e}_r + u_\theta \mathbf{e}_\theta + u_z \mathbf{e}_z. \quad (\text{A } 1)$$

We only consider an inertial frame in this appendix. In addition, we adopt the normalised coordinates and do not distinguish the contravariant and covariant components. We can write the unit vectors of a cylindrical coordinate in Cartesian coordinates as

$$\mathbf{e}_r = \begin{bmatrix} \cos \theta \\ \sin \theta \\ 0 \end{bmatrix}, \quad \mathbf{e}_\theta = \begin{bmatrix} -\sin \theta \\ \cos \theta \\ 0 \end{bmatrix}, \quad \mathbf{e}_z = \begin{bmatrix} 0 \\ 0 \\ 1 \end{bmatrix}. \quad (\text{A } 2)$$

The partial derivatives of them yield nonzero values for

$$\frac{\partial}{\partial \theta} \mathbf{e}_r = \mathbf{e}_\theta, \quad \frac{\partial}{\partial \theta} \mathbf{e}_\theta = -\mathbf{e}_r. \quad (\text{A } 3)$$

Therefore, we have

$$\frac{\partial}{\partial r} \mathbf{u} = \frac{\partial u_r}{\partial r} \mathbf{e}_r + \frac{\partial u_\theta}{\partial r} \mathbf{e}_\theta + \frac{\partial u_z}{\partial r}, \quad (\text{A } 4a)$$

$$\frac{\partial}{\partial \theta} \mathbf{u} = \frac{\partial u_r}{\partial \theta} \mathbf{e}_r + \frac{\partial u_\theta}{\partial \theta} \mathbf{e}_\theta + u_r \mathbf{e}_\theta - u_\theta \mathbf{e}_r + \frac{\partial u_z}{\partial \theta}. \quad (\text{A } 4b)$$

Thus, the covariant form of the velocity gradient tensor in cylindrical coordinates should be

$$\nabla \mathbf{u} = \begin{bmatrix} \nabla_r u_r & \nabla_\theta u_r & \nabla_z u_r \\ \nabla_r u_\theta & \nabla_\theta u_\theta & \nabla_z u_\theta \\ \nabla_r u_z & \nabla_\theta u_z & \nabla_z u_z \end{bmatrix} = \begin{bmatrix} \frac{\partial u_r}{\partial r} & \frac{1}{r} \frac{\partial u_r}{\partial \theta} - \frac{u_\theta}{r} & \frac{\partial u_r}{\partial z} \\ \frac{\partial u_\theta}{\partial r} & \frac{1}{r} \frac{\partial u_\theta}{\partial \theta} + \frac{u_r}{r} & \frac{\partial u_\theta}{\partial z} \\ \frac{\partial u_z}{\partial r} & \frac{1}{r} \frac{\partial u_z}{\partial \theta} & \frac{\partial u_z}{\partial z} \end{bmatrix}. \quad (\text{A } 5)$$

This can be written using the suffix notation as

$$\nabla_j u_i = \frac{\partial u_i}{\partial x_j} + \Gamma_{i\ell,j} u_\ell, \quad (\text{A } 6)$$

where  $(u_1, u_2, u_3) = (u_r, u_\theta, u_z)$  and

$$\frac{\partial}{\partial x_1} = \frac{\partial}{\partial r}, \quad \frac{\partial}{\partial x_2} = \frac{1}{r} \frac{\partial}{\partial \theta}, \quad \frac{\partial}{\partial x_3} = \frac{\partial}{\partial z},$$

$$\Gamma_{i\ell,j} = \mathbf{e}_i \cdot \frac{\partial \mathbf{e}_\ell}{\partial x_j} = \begin{cases} \Gamma_{21,2} = -\Gamma_{12,2} = \frac{1}{r} \\ 0 \end{cases} \quad (\text{otherwise}), \quad (\text{A } 7)$$

with  $(\mathbf{e}_1, \mathbf{e}_2, \mathbf{e}_3) = (\mathbf{e}_r, \mathbf{e}_\theta, \mathbf{e}_z)$ .  $\Gamma_{i\ell,j}$  is the Christoffel symbol in the Euclidean space. Note that this definition of the Christoffel symbol differs from that depicted in (2.4). The definition (2.4) considers the case where  $(x^1, x^2, x^3) = (r, \theta, z)$ , and thus the metric tensor yields  $\{g_{ij}\} = \text{diag}(1, r^2, 1)$  in the cylindrical coordinates; this definition may be suitable for the general formulation of models. However, when we write the equations under this definition of metric tensor  $\{g_{ij}\} = \text{diag}(1, r^2, 1)$ , the contravariant component of the azimuthal velocity  $u^\theta$  will have a dimension of  $[\text{T}^{-1}]$  instead of  $[\text{LT}^{-1}]$ . In contrast, when we adopt the formulation presented in this appendix, the dimension of the azimuthal velocity  $u_\theta$  yields  $[\text{LT}^{-1}]$ . Thus, the formulation using the definition of the Christoffel symbol given by (A 7) may be convenient for deriving the familiar form of basic equations in cylindrical coordinates. The velocity gradient expressed in (A 5) satisfies the rule of orthogonal transformation; namely, the transformation of the velocity gradient tensor between the Cartesian and cylindrical coordinates yields

$$\begin{bmatrix} \frac{\partial u_x}{\partial x} & \frac{\partial u_x}{\partial y} & \frac{\partial u_x}{\partial z} \\ \frac{\partial u_y}{\partial x} & \frac{\partial u_y}{\partial y} & \frac{\partial u_y}{\partial z} \\ \frac{\partial u_z}{\partial x} & \frac{\partial u_z}{\partial y} & \frac{\partial u_z}{\partial z} \end{bmatrix} = \mathbf{O}^t \begin{bmatrix} \nabla_r u_r & \nabla_\theta u_r & \nabla_z u_r \\ \nabla_r u_\theta & \nabla_\theta u_\theta & \nabla_z u_\theta \\ \nabla_r u_z & \nabla_\theta u_z & \nabla_z u_z \end{bmatrix} \mathbf{O}, \quad (\text{A } 8)$$

where  $\mathbf{O}^t$  denotes the transpose of  $\mathbf{O}$ , and  $\mathbf{O}$  is an orthogonal matrix of transformation defined by

$$\mathbf{O}^t = \begin{bmatrix} \frac{\partial x}{\partial r} & \frac{1}{r} \frac{\partial x}{\partial \theta} & \frac{\partial x}{\partial z} \\ \frac{\partial y}{\partial r} & \frac{1}{r} \frac{\partial y}{\partial \theta} & \frac{\partial y}{\partial z} \\ \frac{\partial z}{\partial r} & \frac{1}{r} \frac{\partial z}{\partial \theta} & \frac{\partial z}{\partial z} \end{bmatrix} = \begin{bmatrix} \cos \theta & -\sin \theta & 0 \\ \sin \theta & \cos \theta & 0 \\ 0 & 0 & 1 \end{bmatrix}. \quad (\text{A } 9)$$

Therefore, the velocity gradient expressed in (A 5) transforms as a tensor (for details, see e.g. Thiffeault 2001; Frewer 2009; Ariki 2015a). This calculation rule of a derivative is used for any vector and tensor quantities in cylindrical coordinates. For example, the gradients of the second-rank contravariant tensor  $A_{ij}$  in cylindrical coordinates can be calculated as follows:

$$\nabla_\theta A_{rr} = \frac{1}{r} \frac{\partial A_{rr}}{\partial \theta} + \Gamma_{12,2} A_{\theta r} + \Gamma_{12,2} A_{r\theta} = \frac{1}{r} \frac{\partial A_{rr}}{\partial \theta} - \frac{A_{\theta r}}{r} - \frac{A_{r\theta}}{r}, \quad (\text{A } 10a)$$

$$\nabla_\theta A_{\theta\theta} = \frac{1}{r} \frac{\partial A_{\theta\theta}}{\partial \theta} + \Gamma_{21,2} A_{r\theta} + \Gamma_{21,2} A_{\theta r} = \frac{1}{r} \frac{\partial A_{\theta\theta}}{\partial \theta} + \frac{A_{r\theta}}{r} + \frac{A_{\theta r}}{r}, \quad (\text{A } 10b)$$

$$\nabla_\theta A_{r\theta} = \frac{1}{r} \frac{\partial A_{r\theta}}{\partial \theta} + \Gamma_{12,2} A_{\theta\theta} + \Gamma_{21,2} A_{rr} = \frac{1}{r} \frac{\partial A_{r\theta}}{\partial \theta} - \frac{A_{\theta\theta}}{r} + \frac{A_{rr}}{r}. \quad (\text{A } 10c)$$

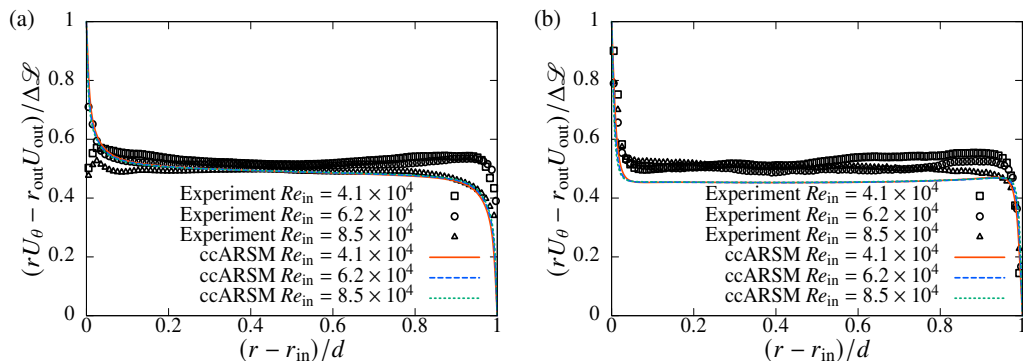


Figure 11: Mean angular momentum profiles of experiments and ccARSM at  $Re_{in} = 4.1 \times 10^4$ ,  $6.2 \times 10^4$ , and  $8.5 \times 10^4$  for (a)  $a = 0$  and (b)  $a = -0.33$ .

$\nabla_j u^i$  is the trace of (A 5). Similarly, the Laplacian of the velocity fields  $g^{i\ell} \nabla_j \nabla_\ell u^i$  can be written as

$$\begin{aligned} g^{i\ell} \nabla_j \nabla_\ell u^i &= \frac{\partial}{\partial x_j} (\nabla_j u_i) + \Gamma_{j\ell,j} \nabla_\ell u_i + \Gamma_{i\ell,j} \nabla_j u_\ell \\ &= \frac{\partial}{\partial x_j} \left( \frac{\partial u_i}{\partial x_j} + \Gamma_{i\ell,j} u_\ell \right) + \Gamma_{j\ell,j} \left( \frac{\partial u_i}{\partial x_\ell} + \Gamma_{im,\ell} u_m \right) + \Gamma_{i\ell,j} \left( \frac{\partial u_\ell}{\partial x_j} + \Gamma_{\ell m,j} u_m \right). \end{aligned} \quad (\text{A } 11)$$

Thus, we have

$$\nabla_j \nabla_j \begin{bmatrix} u_r \\ u_\theta \\ u_z \end{bmatrix} = \begin{bmatrix} \left[ \frac{1}{r} \frac{\partial}{\partial r} \left( r \frac{\partial}{\partial r} \right) + \frac{1}{r^2} \frac{\partial^2}{\partial \theta^2} + \frac{\partial^2}{\partial z^2} \right] u_r - \frac{2}{r^2} \frac{\partial u_\theta}{\partial \theta} - \frac{u_r}{r^2} \\ \left[ \frac{1}{r} \frac{\partial}{\partial r} \left( r \frac{\partial}{\partial r} \right) + \frac{1}{r^2} \frac{\partial^2}{\partial \theta^2} + \frac{\partial^2}{\partial z^2} \right] u_\theta + \frac{2}{r^2} \frac{\partial u_r}{\partial \theta} - \frac{u_\theta}{r^2} \\ \left[ \frac{1}{r} \frac{\partial}{\partial r} \left( r \frac{\partial}{\partial r} \right) + \frac{1}{r^2} \frac{\partial^2}{\partial \theta^2} + \frac{\partial^2}{\partial z^2} \right] u_z \end{bmatrix}, \quad (\text{A } 12)$$

in cylindrical coordinates. The covariant derivative of scalars, e.g. pressure, yields the conventional partial derivative. In cylindrical coordinates, the pressure gradient can be written as follows:

$$(\nabla_r p, \nabla_\theta p, \nabla_z p) = \left( \frac{\partial p}{\partial r}, \frac{1}{r} \frac{\partial p}{\partial \theta}, \frac{\partial p}{\partial z} \right). \quad (\text{A } 13)$$

## Appendix B. Reynolds number dependence of angular momentum

Figure 11 shows the mean angular momentum of the experiments and ccARSM for  $a = 0$  and  $-0.33$  at  $Re = 4.1 \times 10^4$ ,  $6.2 \times 10^4$ , and  $8.5 \times 10^4$ . The experimental results yield almost constant in the bulk region independently of the Reynolds number for both  $a = 0$  and  $a = -0.33$ . For the ccARSM, the profile is independent of the Reynolds number, except for a small difference in the vicinity of the wall. The RANS model is intrinsically independent of the Reynolds number, based on its concept of construction for predicting high-Reynolds-number turbulent flows. Because the bulk region is almost independent of the Reynolds number, the high-Reynolds-number TC turbulence is consistent with the concept of RANS simulation.



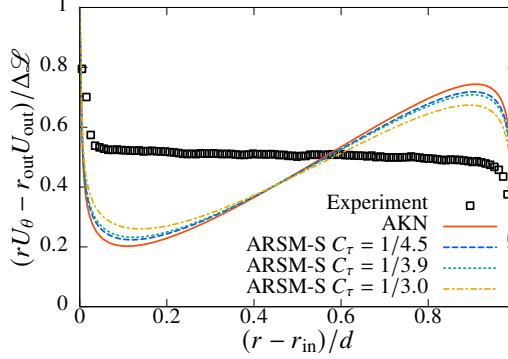


Figure 12: Angular momentum profiles of the AKN (linear eddy viscosity) model and ARSM-S provided by (C 1) at  $Re_{in} = 8.5 \times 10^4$  for  $a = -0.33$ .

### Appendix C. Effect of strain rate for predicting constant angular momentum

To verify the effect of the strain rate in the ARSM (2.52), we consider the following model, similar to (3.9):

$$R_{r\theta} = -\frac{2C_1}{1 + 4\tau_\Gamma^2 C_2^2 S_{r\theta}^2 / 3} \tau_\Gamma K S_{r\theta}, \quad \tau_\Gamma = C_\tau f_\nu \frac{K}{\varepsilon}. \quad (\text{C } 1)$$

We refer to the model (C 1) as the ARSM-S. We also set  $C_2 = 1$  and  $C_1 = C_\nu / C_\tau$  with  $C_\nu$  such that  $C_2 = 0$  leads to the AKN model. In contrast to (2.52), the coefficient of the strain rate in the denominator is positive in (C 1). Several studies have employed this type of modelling (see e.g. Shih *et al.* 1993; Yoshizawa *et al.* 2006).

Figure 12 depicts the mean angular momentum predicted by the AKN (linear eddy viscosity) model and ARSM-S at  $Re_{in} = 8.5 \times 10^4$  for  $a = -0.33$ . As observed in figure 12, the ARSM-S is ineffective in predicting a constant mean angular momentum. Note that for  $C_\tau > 1/3$ , we cannot numerically obtain the relevant mean velocity or angular momentum profile. Consequently, the strain rate in the denominator of the ARSM is not essential for modelling curvature effects.

### Appendix D. Covariant time derivatives: convective and Jaumann derivative

The Oldroyd or convective derivative is a representative covariant time derivative (Oldroyd 1950). The convective derivative of a tensor  $A_{\ell m \dots}^{ij \dots}$  reads

$$\begin{aligned} \frac{\mathfrak{d}A_{\ell m \dots}^{ij \dots}}{\mathfrak{d}t} = & \left( \frac{\partial}{\partial t} + u^a \nabla_a \right) A_{\ell m \dots}^{ij \dots} - (\nabla_a u^i) A_{\ell m \dots}^{aj \dots} - (\nabla_a u^j) A_{\ell m \dots}^{ia \dots} - \dots \\ & + (\nabla_\ell u^a) A_{am \dots}^{ij \dots} + (\nabla_m u^a) A_{\ell a \dots}^{ij \dots} + \dots, \quad (\text{D } 1) \end{aligned}$$

which forms a tensor as it satisfies (1.1). Therefore, even in a rotating frame  $(t^\dagger, \mathbf{x}^\dagger)$ , it reads

$$\begin{aligned} \frac{\mathfrak{d}A_{\ell m \dots}^{\dagger ij \dots}}{\mathfrak{d}t^\dagger} = & \left( \frac{\partial}{\partial t^\dagger} + u^\dagger a \nabla_a^\dagger \right) A_{\ell m \dots}^{\dagger ij \dots} - (\nabla_a^\dagger u^\dagger i) A_{\ell m \dots}^{\dagger aj \dots} - (\nabla_a^\dagger u^\dagger j) A_{\ell m \dots}^{\dagger ia \dots} - \dots \\ & + (\nabla_\ell^\dagger u^\dagger a) A_{am \dots}^{\dagger ij \dots} + (\nabla_m^\dagger u^\dagger a) A_{\ell a \dots}^{\dagger ij \dots} + \dots. \quad (\text{D } 2) \end{aligned}$$

We can construct other covariant derivatives as follows (Thiffeault 2001):

$$\begin{aligned} \mathcal{D}A^{ij\dots}_{\ell m\dots} &= \frac{\mathfrak{d}A^{ij\dots}_{\ell m\dots}}{\mathfrak{d}t} + \mathcal{H}^i_a A^{aj\dots}_{\ell m\dots} + \mathcal{H}^j_a A^{ia\dots}_{\ell m\dots} + \dots \\ &\quad - \mathcal{H}^a_\ell A^{ij\dots}_{am\dots} - \mathcal{H}^a_m A^{ij\dots}_{\ell a\dots} - \dots, \end{aligned} \quad (\text{D } 3)$$

where  $\mathcal{H}^i_j$  is an arbitrary second-rank tensor; thus,  $\mathcal{D}A^{ij\dots}_{\ell m\dots}$  is also a tensor. We employ  $\mathcal{H}^i_j = s^i_j = g^{ia}s_{aj}$ . The strain-rate tensor  $s_{ij}$  is defined in general coordinates as (Oldroyd 1950; Thiffeault 2001; Ariki 2015a)

$$s_{ij} = \frac{1}{2} \frac{\mathfrak{d}g_{ij}}{\mathfrak{d}t} = \frac{1}{2} \left( \frac{\partial g_{ij}}{\partial t} + \nabla_i u_j + \nabla_j u_i \right), \quad (\text{D } 4)$$

where  $g_{ij}$  is a metric tensor, and we use  $\nabla_a g_{ij} = 0$ . The ensemble average of this strain rate is identical to (2.20) with (2.21) (Ariki 2015a). Then,  $\mathcal{D}A^{ij\dots}_{\ell m\dots}$  yields the Jaumann derivative (Oldroyd 1958; Thiffeault 2001):

$$\begin{aligned} \frac{dA^{ij\dots}_{\ell m\dots}}{dt} &= \frac{\mathfrak{d}A^{ij\dots}_{\ell m\dots}}{\mathfrak{d}t} + s^i_a A^{aj\dots}_{\ell m\dots} + s^j_a A^{ia\dots}_{\ell m\dots} + \dots \\ &\quad - s^a_\ell A^{ij\dots}_{am\dots} - s^a_m A^{ij\dots}_{\ell a\dots} - \dots. \end{aligned} \quad (\text{D } 5)$$

This is often referred to as the corotational derivative (Thiffeault 2001) after its form in the frame where the metric is time-independent:

$$\begin{aligned} \frac{dA^{ij\dots}_{\ell m\dots}}{dt} &= \left( \frac{\partial}{\partial t} + u^a \nabla_a \right) A^{ij\dots}_{\ell m\dots} - w^i_a A^{aj\dots}_{\ell m\dots} - w^j_a A^{ia\dots}_{\ell m\dots} - \dots \\ &\quad - w^a_\ell A^{ij\dots}_{am\dots} - w^a_m A^{ij\dots}_{\ell a\dots} - \dots, \end{aligned} \quad (\text{D } 6)$$

where  $w^i_j = g^{ia}w_{aj}$ ,  $w^j_i = g^{ja}w_{ia}$ , and  $w_{ij} = (\nabla_j u_i - \nabla_i u_j)/2$ . Thus, the Jaumann derivative in the inertial frame along with the mean velocity yields (4.1). In a general coordinate, the strain-rate tensor is defined by the Oldroyd derivative of the metric tensor, which generally involves the partial time derivative of the metric tensor (see e.g. Thiffeault 2001; Ariki 2015a). Therefore, the Jaumann derivative is not always written by  $w_{ij}$  as in (D 5). Additionally, for a rotating frame  $(t^\dagger, \mathbf{x}^\dagger)$  with a time-independent metric, the strain rate reads  $s^\dagger_{ij} = (\nabla^\dagger_j u^\dagger_i + \nabla^\dagger_i u^\dagger_j)/2$ ; thus, the Jaumann derivative yields

$$\begin{aligned} \frac{dA^\dagger{}^{ij\dots}_{\ell m\dots}}{dt^\dagger} &= \left( \frac{\partial}{\partial t^\dagger} + u^\dagger{}^a \nabla^\dagger{}_a \right) A^\dagger{}^{ij\dots}_{\ell m\dots} - w^\dagger{}^i_a A^\dagger{}^{aj\dots}_{\ell m\dots} - w^\dagger{}^j_a A^\dagger{}^{ia\dots}_{\ell m\dots} - \dots \\ &\quad - w^\dagger{}^a_\ell A^\dagger{}^{ij\dots}_{am\dots} - w^\dagger{}^a_m A^\dagger{}^{ij\dots}_{\ell a\dots} - \dots, \end{aligned} \quad (\text{D } 7)$$

where  $w^\dagger{}_{ij}$  is not the absolute vorticity, but the conventional vorticity  $w^\dagger{}_{ij} = (\nabla^\dagger{}_j u^\dagger{}_i - \nabla^\dagger{}_i u^\dagger{}_j)/2$  as defined in (2.46).

## REFERENCES

- ABE, H. 2019 Direct numerical simulation of a turbulent boundary layer with separation and reattachment over a range of Reynolds numbers. *Fluid Dyn. Res.* **51**, 011409.
- ABE, K., KONDOH, T. & NAGANO, Y. 1994 A new turbulence model for predicting fluid flow and heat transfer in separating and reattaching flows-I. Flow field calculations. *Int. J. Heat Mass Transfer* **37**, 139–151.

- AHMADI, G. & CHOWDHURY, S. J. 1991 A rate-dependent algebraic stress model for turbulence. *Appl. Math. Modelling* **15**, 516–524.
- ANDERECK, C. D., LIU, S. S. & SWINNEY, H. L. 1986 Flow regimes in a circular Couette system with independently rotating cylinders. *J. Fluid Mech.* **164**, 155–183.
- ARIKI, T. 2015a Covariance of fluid-turbulence theory. *Phys. Rev. E* **91**, 053001.
- ARIKI, T. 2015b Turbulence constitutive modeling of the square root of the Reynolds stress. *Phys. Rev. E* **92**, 053010.
- ARIKI, T. 2017 Mean-Lagrangian formalism and covariance of fluid turbulence. *Phys. Rev. E* **95**, 053102.
- ARIKI, T. 2019 Constitutive theory of inhomogeneous turbulent flow based on two-scale Lagrangian formalism. *Phys. Fluids* **31**, 065104.
- ARIKI, T. & IKEDA, M. 2023 Reynolds-stress root modeling based on a statistical theory. *Phys. Fluids* **35**, 085109.
- BERGHOUT, P., VERZICCO, R., STEVENS, R. J. A. M., LOHSE, D. & CHUNG, D. 2020 Calculation of the mean velocity profile for strongly turbulent Taylor–Couette flow at arbitrary radius ratios. *J. Fluid Mech.* **905**, A11.
- BRAUCKMANN, H. J. & ECKHARDT, B. 2013 Direct numerical simulations of local and global torque in Taylor–Couette flow up to  $Re = 30000$ . *J. Fluid Mech.* **718**, 398–427.
- BRAUCKMANN, H. J., SALEWSKI, M. & ECKHARDT, B. 2016 Momentum transport in Taylor–Couette flow with vanishing curvature. *J. Fluid Mech.* **790**, 419–452.
- BRETHOUWER, G. 2022 Turbulent flow in curved channels. *J. Fluid Mech.* **931**, A21.
- CAMBON, C., BENOIT, J.-P., SHAO, L. & JACQUIN, L. 1994 Stability analysis and large-eddy simulation of rotating turbulence with organized eddies. *J. Fluid Mech.* **278**, 175–200.
- CHENG, W., PULLIN, D. I. & SAMTANEY, R. 2020 Large-eddy simulation and modelling of Taylor–Couette flow. *J. Fluid Mech.* **890**, A17.
- CHOSSAT, P. & IOOSS, G. 1994 *The Couette–Taylor Problem*. Springer New York, NY.
- CHOUPIPE, A., CLIMENT, E., LEGENDRE, D. & GABILLET, C. 2014 Numerical simulation of bubble dispersion in turbulent Taylor–Couette flow. *Phys. Fluids* **26**, 043304.
- COLES, D. 1965 Transition in circular couette flow. *J. Fluid Mech.* **21**, 385–425.
- CRAFT, T. J., LAUNDER, B. E. & SUGA, K. 1996 Development and application of a cubic eddy-viscosity model of turbulence. *Int. J. Heat Fluid Flow* **17**, 108–115.
- DEGUCHI, K. 2023 On high-Taylor-number Taylor vortices. *J. Fluid Mech.* **967**, A11.
- DONG, S. 2007 Direct numerical simulation of turbulent Taylor–Couette flow. *J. Fluid Mech.* **587**, 373–393.
- DUBRULLE, B., DAUCHOT, O., DAVIAUD, F., LONGARETTI, P.-Y., RICHARD, D. & ZAHN, J.-P. 2005 Stability and turbulent transport in Taylor–Couette flow from analysis of experimental data. *Phys. Fluids* **17**, 095103.
- DURAISAMY, K., IACCARINO, G. & XIAO, H. 2019 Turbulence modeling in the age of data. *Annu. Rev. Fluid Mech.* **51**, 357–377.
- DURBIN, P. A. 2018 Some recent developments in turbulence closure modeling. *Annu. Rev. Fluid Mech.* **50**, 77–103.
- ECKHARDT, B., GROSSMANN, S. & LOHSE, D. 2007 Torque scaling in turbulent Taylor–Couette flow between independently rotating cylinders. *J. Fluid Mech.* **581**, 221–250.
- EZETA, R., HUISMAN, S. G., SUN, C. & LOHSE, D. 2018 Turbulence strength in ultimate Taylor–Couette turbulence. *J. Fluid Mech.* **836**, 397–412.
- FREWER, M. 2009 More clarity on the concept of material frame-indifference in classical continuum mechanics. *Acta Mech.* **202**, 213–246.
- FROITZHEIM, A., MERBOLD, S. & EGBERS, C. 2017 Velocity profiles, flow structures and scalings in a wide-gap turbulent Taylor–Couette flow. *J. Fluid Mech.* **831**, 330–357.
- FROITZHEIM, A., MERBOLD, S., OSTILLA-MÓNICO, R. & EGBERS, C. 2019 Angular momentum transport and flow organization in Taylor–Couette flow at radius ratio of  $\eta = 0.357$ . *Phys. Rev. Fluids* **4**, 084605.
- GATSKI, T. B. & JONGEN, T. 2000 Nonlinear eddy viscosity and algebraic stress models for solving complex turbulent flows. *Prog. Aerospace Sci.* **36**, 655–682.
- GATSKI, T. B. & SPEZIALE, C. G. 1993 On explicit algebraic stress models for complex turbulent flows. *J. Fluid Mech.* **254**, 59–78.
- GATSKI, T. B. & WALLIN, S. 2004 Extending the weak-equilibrium condition for algebraic Reynolds stress models to rotating and curved flows. *J. Fluid Mech.* **518**, 147–155.

- GIRIMAJI, S. S. 1996 Fully explicit and self-consistent algebraic Reynolds stress model. *Theoret. Comput. Fluid Dyn.* **8**, 387–402.
- GIRIMAJI, S. S. 1997 A Galilean invariant explicit algebraic Reynolds stress model for turbulent curved flows. *Phys. Fluids* **9**, 1067–1077.
- GODDARD, J. D. & MILLER, C. 1966 An inverse for the Jaumann derivative and some applications to the rheology of viscoelastic fluids. *Rheologica Acta* **5**, 177–184.
- GROSSMANN, S., LOHSE, D. & SUN, C. 2016 High-Reynolds number Taylor-Couette turbulence. *Annu. Rev. Fluid Mech.* **48**, 53–80.
- GRUNDESTAM, O., WALLIN, S. & JOHANSSON, A. V. 2008 Direct numerical simulations of rotating turbulent channel flow. *J. Fluid Mech.* **598**, 177–199.
- HAMBA, F. 2006a Euclidean invariance and weak-equilibrium condition for the algebraic Reynolds stress model. *J. Fluid Mech.* **569**, 399–408.
- HAMBA, F. 2006b The mechanism of zero mean absolute vorticity state in rotating channel flow. *Phys. Fluids* **18**, 125104.
- HAMBA, F. 2017 History effect on the Reynolds stress in turbulent swirling flow. *Phys. Fluids* **29**, 025103.
- HAMLINGTON, P. E. & DAHM, W. J. A. 2008 Reynolds stress closure for nonequilibrium effects in turbulent flows. *Phys. Fluids* **20**, 115101.
- HANJALIĆ, K. & LAUNDER, B. 2011 *Modelling Turbulence in Engineering and the Environment: Second-Moment Routes to Closure*. Cambridge: Cambridge University Press.
- HORIE, M. & MITSUME, N. 2024 Graph neural PDE solvers with conservation and similarity-equivariance. In *Forty-first International Conference on Machine Learning*.
- HORIMOTO, Y. & OKUYAMA, H. 2025 Angular momentum transport in Taylor-Couette turbulence of dilute surfactant solution. *Appl. Therm. Eng.* **262**, 125238.
- VAN HOUT, R. & KATZ, J. 2011 Measurements of mean flow and turbulence characteristics in high-Reynolds number counter-rotating Taylor-Couette flow. *Phys. Fluids* **23**, 105102.
- HUISMAN, S. G., SCHARNOWSKI, S., CIERPKA, C., KÄHLER, C. J., LOHSE, D. & SUN, C. 2013 Logarithmic boundary layers in strong Taylor-Couette turbulence. *Phys. Rev. Lett.* **110**, 264501.
- IMAO, S., ITOH, M. & HARADA, T. 1996 Turbulent characteristics of the flow in an axially rotating pipe. *Int. J. Heat Fluid Flow* **17**, 444–451.
- INAGAKI, K., ARIKI, T. & HAMBA, F. 2019 Higher-order realizable algebraic Reynolds stress modeling based on the square root tensor. *Phys. Rev. Fluids* **4**, 114601.
- Ji, H. & BALBUS, S. 2013 Angular momentum transport in astrophysics and in the lab. *Phys. Today* **66**, 27–33.
- JIANG, C., VINUESA, R., CHEN, R., MI, J., LAIMA, S. & LI, H. 2021 An interpretable framework of data-driven turbulence modeling using deep neural networks. *Phys. Fluids* **33**, 055133.
- JOHNSTON, J. P., HALLEEN, R. M. & LEZIUS, D. K. 1972 Effects of spanwise rotation on the structure of two-dimensional fully developed turbulent channel flow. *J. Fluid Mech.* **56**, 533–557.
- KAJISHIMA, T. & TAIRA, K. 2017 *Computational Fluid Dynamics*. New York: Springer.
- KAWATA, T. & ALFREDSSON, P. H. 2016a Experiments in rotating plane Couette flow—momentum transport by coherent roll-cell structure and zero-absolute-vorticity state. *J. Fluid Mech.* **791**, 191–213.
- KAWATA, T. & ALFREDSSON, P. H. 2016b Turbulent rotating plane Couette flow: Reynolds and rotation number dependency of flow structure and momentum transport. *Phys. Rev. Fluids* **1**, 034402.
- LANDAU, L. D. & LIFSHITZ, E. M. 1975 *The Classical Theory of Fields, Course of Theoretical Physics Vol. 2*. Oxford: Butterworth-Heinemann.
- LAUNDER, B. E., REECE, G. J. & RODI, W. 1975 Progress in the development of a Reynolds-stress turbulence closure. *J. Fluid Mech.* **68**, 537–566.
- LEWIS, G. S. & SWINNEY, H. L. 1999 Velocity structure functions, scaling, and transitions in high-Reynolds-number Couette-Taylor flow. *Phys. Rev. E* **59**, 5457–5467.
- LING, J., KURZAWSKI, A. & TEMPLETON, J. 2016 Reynolds averaged turbulence modelling using deep neural networks with embedded invariance. *J. Fluid Mech.* **807**, 155–166.
- MISHRA, A. A. & GIRIMAJI, S. S. 2014 On the realizability of pressure-strain closures. *J. Fluid Mech.* **755**, 535–560.
- NAGATA, M. & KASAGI, N. 2004 Spatio-temporal evolution of coherent vortices in wall turbulence with streamline curvature. *J. Turbulence* **5**, 917.
- OLDROYD, J. G. 1950 On the formulation of rheological equations of state. *Proc. Roy. Soc. A* **200**, 523–541.

- OLDROYD, J. G. 1958 Non-Newtonian effects in steady motion of some idealized elastico-viscous liquids. *Proc. Roy. Soc. A* **245**, 278–297.
- ORLANDI, P. & FATICA, M. 1997 Direct simulations of turbulent flow in a pipe rotating about its axis. *J. Fluid Mech.* **343**, 43–72.
- OSTILLA-MÓNICO, R., VAN DER POEL, E. P., VERZICCO, R., GROSSMANN, S. & LOHSE, D. 2014a Boundary layer dynamics at the transition between the classical and the ultimate regime of Taylor–Couette flow. *Phys. Fluids* **26**, 015114.
- OSTILLA-MÓNICO, R., STEVENS, R. J. A. M., GROSSMANN, S., VERZICCO, R. & LOHSE, D. 2014b Optimal Taylor–Couette flow: direct numerical simulations. *J. Fluid Mech.* **719**, 14–46.
- OSTILLA-MÓNICO, R., VAN DER POEL, E. P., VERZICCO, R., GROSSMANN, S. & LOHSE, D. 2014c Exploring the phase diagram of fully turbulent Taylor–Couette flow. *J. Fluid Mech.* **761**, 1–26.
- POPE, S. B. 1975 A more general effective-viscosity hypothesis. *J. Fluid Mech.* **72**, 331–340.
- POPE, S. B. 2000 *Turbulent Flows*. Cambridge: Cambridge University Press.
- RAYLEIGH, L. 1917 On the dynamics of revolving fluids. *Proc. R. Soc. London, Ser. A* **93**, 148–154.
- SCHARTMAN, E., JI, H. & BURIN, M. J. 2009 Development of a Couette–Taylor flow device with active minimization of secondary circulation. *Rev. Sci. Instrum.* **80** (2), 024501.
- SCHUMANN, U. 1977 Realizability of Reynolds-stress turbulence models. *Phys. Fluids* **20**, 721–725.
- SHIH, T.-H., ZHU, J. & LUMLEY, J. L. 1993 A realizable Reynolds stress algebraic equation model. *NASA TM 105993*.
- SMITH, G. P. & TOWNSEND, A. A. 1982 Turbulent Couette flow between concentric cylinders at large Taylor numbers. *J. Fluid Mech.* **123**, 187–217.
- SPALART, P. R. & SHUR, M. 1997 On the sensitization of turbulence models to rotation and curvature. *Aerosp. Sci. Technol.* **5**, 297–302.
- SPEZIALE, C. G. 1979 Invariance of turbulent closure models. *Phys. Fluids* **22**, 1033–1037.
- SPEZIALE, C. G. 1987 On nonlinear  $K-l$  and  $K-\epsilon$  models of turbulence. *J. Fluid Mech.* **178**, 459–475.
- SPEZIALE, C. G., YOUNIS, B. A. & BERGER, S. A. 2000 Analysis and modelling of turbulent flow in an axially rotating pipe. *J. Fluid Mech.* **407**, 1–26.
- TANAKA, M., KIDA, S., YANASE, S. & KAWAHARA, G. 2000 Zero-absolute-vorticity state in a rotating turbulent shear flow. *Phys. Fluids* **12** (8), 1979–1985.
- TAULBEE, D. B. 1992 An improved algebraic Reynolds stress model and corresponding nonlinear stress model. *Phys. Fluids A* **4**, 2555–2561.
- THIFFEAULT, J.-L. 2001 Covariant time derivatives for dynamical systems. *J. Phys. A: Math. Gen.* **34**, 5875–5885.
- WALLIN, S. & JOHANSSON, A. V. 2000 An explicit algebraic Reynolds stress model for incompressible and compressible turbulent flows. *J. Fluid Mech.* **403**, 89–132.
- WALLIN, S. & JOHANSSON, A. V. 2002 Modelling streamline curvature effects in explicit algebraic Reynolds stress turbulence models. *Int. J. Heat Fluid Flow* **23**, 721–730.
- WATTENDORF, F. L. 1935 A study of the effect of curvature on fully developed turbulent flow. *Proc. R. Soc. A* **148**, 565–598.
- WEIS, J. & HUTTER, K. 2003 On Euclidean invariance of algebraic Reynolds stress models in turbulence. *J. Fluid Mech.* **476**, 63–68.
- WENDT, F. 1933 Turbulente strömungen zwischen zwei rotierenden konaxialen zylindern. *Ingenieur-Archiv* **4**, 577–595.
- WU, J.-L., XIAO, H. & PATERSON, E. 2018 Physics-informed machine learning approach for augmenting turbulence models: A comprehensive framework. *Phys. Rev. Fluids* **3**, 074602.
- XIA, Z., SHI, Y. & CHEN, S. 2016 Direct numerical simulation of turbulent channel flow with spanwise rotation. *J. Fluid Mech.* **788**, 42–56.
- YOSHIZAWA, A. 1984 Statistical analysis of the derivation of the Reynolds stress from its eddy-viscosity representation. *Phys. Fluids* **27**, 1377–1387.
- YOSHIZAWA, A. 1998 *Hydrodynamic and Magnetohydrodynamic Turbulent Flows: Modelling and Statistical Theory*. Dordrecht: Kluwer.
- YOSHIZAWA, A., NISIZIMA, S., SHIMOMURA, Y., KOBAYASHI, H., MATSUO, Y., ABE, H. & FUJIWARA, H. 2006 A new methodology for Reynolds-averaged modeling based on the amalgamation of heuristic-modeling and turbulence-theory methods. *Phys. Fluids* **18**, 035109.
- YU, D. & GIRIMAJI, S. S. 2006 Direct numerical simulations of homogeneous turbulence subject to periodic shear. *J. Fluid Mech.* **566**, 117–151.